J|A|C|S
ARTICLES
Published on Web 06/01/2002

Theoretical Study of Rhodium(III)-Catalyzed Hydrogenation of Carbon Dioxide into Formic Acid. Significant Differences in Reactivity among Rhodium(III), Rhodium(I), and Ruthenium(II) Complexes

Yasuo Musashi*,† and Shigeyoshi Sakaki*,‡

Contribution from the Information Processing Center, Kumamoto University, Kumamoto 860-8555, Japan, and Institute for Fundamental Research of Organic Chemistry, Kyushu University, Higashi-ku, Hakozaki 812-8581, Japan

Received January 10, 2002

Abstract: The title reaction was theoretically investigated, where *cis*-$[RhH_2(PH_3)_3]^+$ and *cis*-$[RhH_2(PH_3)_2(H_2O)]^+$ were adopted as models of the catalyst. The first step of the catalytic cycle is the CO_2 insertion into the Rh(III)−H bond, of which the activation barrier (E_a) is 47.2 and 28.4 kcal/mol in *cis*-$[RhH_2(PH_3)_3]^+$ and *cis*-$[RhH_2(PH_3)_2(H_2O)]^+$, respectively, where DFT(B3LYP)-calculated E_a values (kcal/mol unit) are given hereafter. These results indicate that an active species is not *cis*-$[RhH_2(PH_3)_3]^+$ but *cis*-$[RhH_2(PH_3)_2(H_2O)]^+$. After the CO_2 insertion, two reaction courses are possible. In one course, the reaction proceeds through isomerization ($E_a = 2.8$) of $[RhH(\eta^1\text{-}OCOH)(PH_3)_2(H_2O)_2]^+$, five-centered H−OCOH reductive elimination ($E_a = 2.7$), and oxidative addition of H_2 to $[Rh(PH_3)_2(H_2O)_2]^+$ ($E_a = 5.8$). In the other one, the reaction proceeds through isomerization of $[RhH(\eta^1\text{-}OCOH)(PH_3)_2(H_2O)(H_2)]^+$ ($E_a = 5.9$) and six-centered σ-bond metathesis of $[RhH(\eta^1\text{-}OCOH)(PH_3)_2(H_2O)]^+$ with H_2 (no barrier). $RhH(PH_3)_2$-catalyzed hydrogenation of CO_2 proceeds through CO_2 insertion ($E_a = 1.6$) and either the isomerization of $Rh(\eta^1\text{-}OCOH)(PH_3)_2(H_2)$ ($E_a = 6.1$) followed by the six-centered σ-bond metathesis ($E_a = 0.3$) or H_2 oxidative addition to $Rh(\eta^1\text{-}OCOH)(PH_3)_2$ ($E_a = 7.3$) followed by isomerization of $RhH_2(\eta^1\text{-}OCOH)(PH_3)_2$ ($E_a = 6.2$) and the five-centered H−OCOH reductive elimination ($E_a = 1.9$). From these results and our previous results of $RuH_2(PH_3)_4$-catalyzed hydrogenation of CO_2 (*J. Am. Chem. Soc.* **2000**, *122*, 3867), detailed discussion is presented concerning differences among Rh(III), Rh(I), and Ru(II) complexes.

1. Introduction

Carbon dioxide (CO_2) is an abundant, nontoxic, and inexpensive feedstock. To utilize CO_2, however, we need to convert CO_2 into more reactive compounds. The transition metal-catalyzed hydrogenation of CO_2 into formic acid is attractive CO_2 conversion reaction,[2−5] because formic acid is one of raw materials in organic transformations. This reaction is catalyzed by transition metal complexes such as $TiCl_4$,[6] $[WH(CO)_5]^-$,[7] $Pd(dppe)_2$ (dppe = 1,2-bis(diphenylphosphino)ethane),[8] $PdCl_2(PPh_3)_2$,[9] $RhH(P-P)_2$ (P−P = $Ph_2P(CH_2)_nPPh_2$),[10] $[RhH_2(PMe_2Ph)_3(Sol)]BF_4$ (Sol = solvent molecule),[11] $RuH_2(PPh_3)_4$,[8] and $RuH_2(PMe_3)_4$.[12] In the hydrogenation of CO_2 into formic acid with $[Rh(nbd)(PMe_2Ph)_3]BF_4$ (nbd = norbornadiene),[11] a cationic rhodium(III) dihydride complex, $[RhH_2(PMe_2Ph)_3(Sol)]^+$ (Sol = THF or H_2O), and rhodium(III) formate hydride complexes, $[RhH(\eta^1\text{-}OCOH)(PMe_2Ph)_3(Sol)]^+$ and $[RhH(\eta^2\text{-}O_2CH)(PMe_2Ph)_n(Sol)_{4-n}]^+$ ($n = 2$ or 3), were spectroscopically detected. From these results, the catalytic cycle shown in Scheme 1 was proposed,[11] which consists of CO_2 insertion into the Rh(III)−H bond of the rhodium(III) dihydride complex to yield a rhodium(III) formate hydride complex, reductive elimination of formic acid from the rhodium(III) formate hydride complex to yield a rhodium(I) complex, and oxidative addition of molecular dihydrogen to the rhodium(I) complex to regenerate the rhodium(III) dihydride complex.[11] In the hydrogenation of CO_2 into formic acid with RhH(dppp) (dppp = 1,3-bis(diphenylphosphino)propane), however, a slightly different reaction mechanism was theoretically proposed,[13] as shown in

† Kumamoto University.
‡ Kyushu University.

(1) Behr, A. *Carbon Dioxide Activation by Metal Complex*; VCH Publishers: Weinheim, Germany, 1988.
(2) Jessop, P. G.; Morris, R. H. *Coord. Chem. Rev.* **1992**, *121*, 155.
(3) Jessop, P. G.; Ikariya, T.; Noyori, R. *Chem. Rev.* **1995**, *95*, 259.
(4) (a) Leitner, W. *Angew. Chem., Int. Ed. Engl.* **1995**, *34*, 2207. (b) Leitner, W. *Coord. Chem. Rev.* **1996**, *153*, 257.
(5) Kröcher, O.; Köppel, R. A.; Baiker, A. *Chem. Commun.* **1997**, 453.
(6) Jezowska-Trzebiatowska, B.; Sobota, P. *J. Organomet. Chem.* **1974**, *80*, C27.
(7) Darensbourg, D. J.; Ovalles, C. *J. Am. Chem. Soc.* **1984**, *106*, 3750.
(8) Inoue, Y.; Izumida, H.; Sasaki, Y.; Hashimoto, H. *Chem. Lett.* **1976**, 863.
(9) Sakamoto, M.; Shimizu, I.; Yamamoto, A. *Organometallics* **1994**, *13*, 407.
(10) (a) Burgemeister, T.; Kastner, F.; Leitner, W. *Angew. Chem., Int. Ed. Engl.* **1993**, *32*, 739. (b) Leitner, W.; Dinjus, E.; Gassner, F. *J. Organomet. Chem.* **1994**, *475*, 257. (c) Gassner, F.; Leitner, W. *J. Chem. Soc., Chem. Commun.* **1993**, 1465. (d) Fornika, R.; Görls, H.; Seemann, B.; Leitner, W. *J. Chem. Soc., Chem. Commun.* **1995**, 1479.
(11) Tsai, J.-C.; Nicholas, K. M. *J. Am. Chem. Soc.* **1992**, *114*, 5117.
(12) (a) Jessop, P. G.; Ikariya, T.; Noyori, R. *Nature* **1994**, *368*, 231. (b) Jessop, P. G.; Ikariya, T.; Noyori, R. *Science* **1995**, *269*, 1065. (c) Jessop, P. G.; Hsiao, Y.; Ikariya, T.; Noyori, R. *J. Am. Chem. Soc.* **1996**, *118*, 344.
(13) (a) Hutschka, F.; Dedieu, A.; Eichberger, M.; Fornika, R.; Leitner, W. *J. Am. Chem. Soc.* **1997**, *119*, 4432. (b) Hutschka, F.; Dedieu, A. *J. Chem. Soc., Dalton Trans.* **1997**, 1899.

10.1021/ja020063c CCC: $22.00

Scheme 1

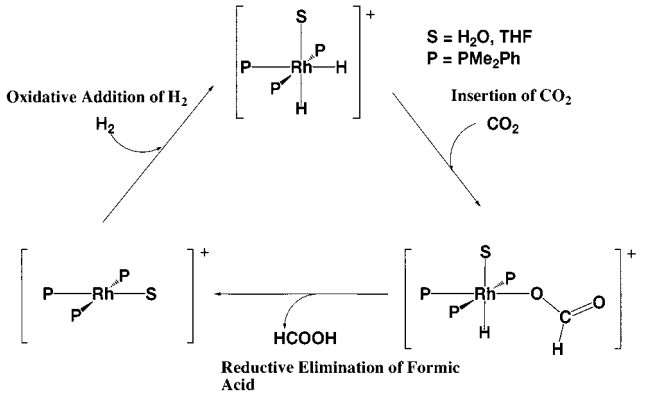

Scheme 2

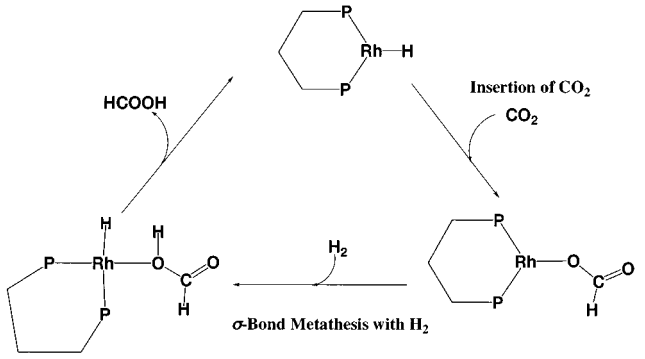

Scheme 2, in which CO_2 is inserted into the Rh(I)−H bond of $RhH(PR_3)_2$ followed by σ-bond metathesis of a rhodium(I) formate complex, $Rh(\eta^1\text{-}OCOH)(PR_3)_2$, with molecular dihydrogen. The release of HCOOH from $Rh(PH_3)_2(HCOOH)$, which is the final step of hydrogenation of CO_2, was also investigated with the DFT-SCRF method.[14] Recently, Jessop, Ikariya, and Noyori reported that $RuX_2(PMe_3)_4$ (X = H and Cl) and $RuCl(\eta^1\text{-}OCOCH_3)(PMe_3)_4$ effciently catalyzed hydrogenation of CO_2 into formic acid in supercritical CO_2.[12c] We theoretically investigated this ruthenium(II)-catalyzed hydrogenation of CO_2 into formic acid and found that this reaction proceeded through CO_2 insertion into the Ru(II)−H bond followed by six-centered σ-bond metathesis of a ruthenium(II) formate hydride complex with molecular dihydrogen.[15]

It is considerably interesting to make comparisons among rhodium(I), rhodium(III), and ruthenium(II) complexes in hydrogenation of CO_2 into formic acid, since they are different in d electron number and oxidation state, as follows: Rhodium(I) takes a d^8 electron configuration with +1 formal oxidation state, rhodium(III) takes a d^6 electron configuration with +3 formal oxidation state, and ruthenium(II) takes a d^6 electron configuration with +2 formal oxidation state. Their d orbitals would be different in energy, which would lead to significant differences in catalysis for the hydrogenation of CO_2.

In this work, we theoretically investigated all the possible elementary steps in the Rh(III)-catalyzed CO_2 hydrogenation reaction, such as insertion of CO_2 into the Rh(III)−H bond (eq 1), H−OCOH reductive elimination from the rhodium(III) formate hydride complex (eq 2), σ-bond metathesis of the rhodium(III) formate hydride complex with molecular dihydrogen (eq 3), and oxidative addition of molecular dihydrogen to $[Rh(PH_3)_2(L)_n(HCOOH)]^+$ (eq 4), where L is either PH_3 or H_2O. We examined here both three-centered transition state (TS) and five-centered TS in the reductive elimination of formic acid and both four-centered TS and six-centered one in the σ-bond metathesis, as shown in Chart 1. This is because all these TS structures are considered possible. In particular, the six-centered σ-bond metathesis is worthy of investigation, because the six-centered H_2 splitting assisted by a ligand was proposed by Darensbourg et al.,[7] Morris et al.,[16] Crabtree et al.,[17] and Milet et al.[18] Our purposes here are (1) to elucidate the reaction mechanism of rhodium(III)-catalyzed hydrogenation of CO_2 into formic acid, (2) to clarify the rate-determining step in the catalytic cycle, and (3) to compare the rhodium(III)-catalyzed CO_2 hydrogenation reaction with rhodium(I)- and ruthenium(II)-catalyzed CO_2 hydrogenation reactions. Our intentions here are to present a deep understanding of the rhodium(III)-catalyzed hydrogenation of CO_2 into formic acid, to specify differences in catalytic cycles among rhodium(III), rhodium(I), and ruthenium(II) catalysts, and to clarify the reasons for the differences.

Chart 1

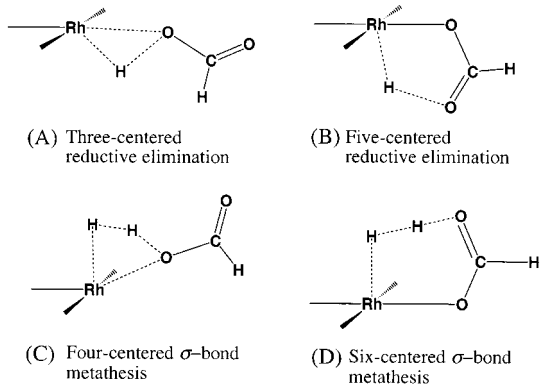

$$cis\text{-}[RhH_2(PH_3)_2(L)]^+ + CO_2 \rightarrow cis\text{-}[RhH(\eta^1\text{-}OCOH)(PH_3)_2(L)]^+ \quad (1)$$

$$cis\text{-}[RhH(\eta^1\text{-}OCOH)(PH_3)_2(L)_n]^+ \rightarrow [Rh(PH_3)_2(L)_n(HCOOH)]^+ \quad (2)$$

$$cis\text{-}[RhH(\eta^1\text{-}OCOH)(PH_3)_2(L)]^+ + H_2 \rightarrow cis\text{-}[RhH_2(PH_3)_2(L)(HCOOH)]^+ \quad (3)$$

$$[Rh(PH_3)_2(L)_n(HCOOH)]^+ + H_2 \rightarrow cis\text{-}[RhH_2(PH_3)_2(L)_n(HCOOH)]^+ \quad (4)$$

$$(L = PH_3 \text{ or } H_2O;\ n = 1 \text{ or } 2)$$

2. Model of the Catalyst and Computations

$[RhH_2(PH_3)_2(L)_2]^+$ (L = PH_3 or H_2O) was adopted here as a model of an active species, considering that Tsai and Nicholas[11] detected *cis*-$[RhH_2(PMe_2Ph)_n(Sol)_{4-n}]^+$ (Sol = THF or H_2O) in the CO_2 hydrogena-

(14) Pomelli, C. S.; Tomasi, J.; Solà, M. *Organometallics* **1998**, *17*, 3164.
(15) Musashi, Y.; Sakaki, S. *J. Am. Chem. Soc.* **2000**, *122*, 3867.
(16) (a) Park, S.; Ramachandran, R.; Lough, A. J.; Morris, R. H. *J. Chem. Soc., Chem. Commun.* **1994**, 2201. (b) Lough, A. J.; Park, S.; Ramachandran, R.; Morris, R. H. *J. Am. Chem. Soc.* **1994**, *116*, 8356.

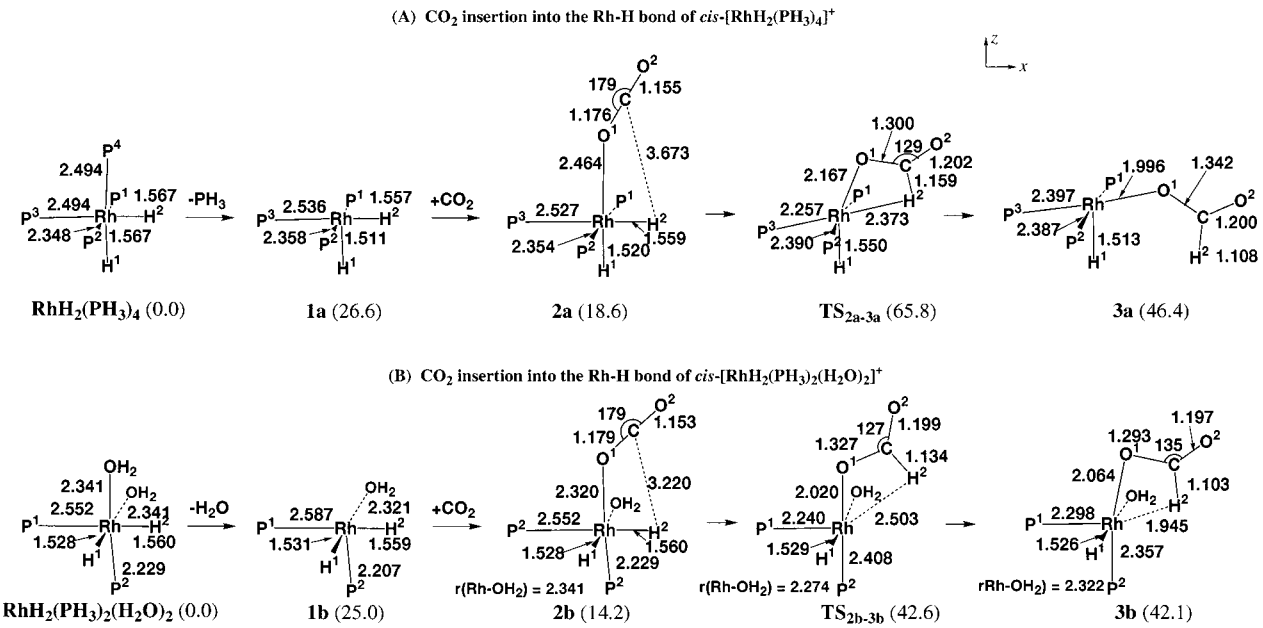

Figure 1. Geometry changes in the insertion of CO_2 into the Rh(III)−H bond of *cis*-$[RhH_2(PH_3)_2(L)_2]^+$ (L = PH_3 or H_2O). Bond distances are in Å, and bond angles are in deg. In parentheses are the energy differences from the reactants, *cis*-$[RhH_2(PH_3)_2(L)_2]^+ + CO_2$ (kcal/mol unit; the DFT(B3LYP)/BS-II//DFT(B3LYP)/BS-I calculation).

tion reaction with $[Rh(nbd)(PMe_2Ph)_3]^+$. We employed PH_3 as a model of dimethylphenylphosphine (PMe_2Ph) and H_2O as a model of solvent because the hydrogenation reaction was carried out in dry THF and wet THF (0.4% H_2O) solutions.[11]

The density functional theory (DFT)[20] was used here with the B3LYP functional for exchange correlation term.[21,22] Geometries were optimized with the following basis set system (BS-I): Core electrons of P (up to 2p) and Rh (up to 3d) were replaced with effective core potentials (ECPs), and their valence electrons were represented with (21/21/1) and (311/311/211) sets, respectively.[23,24] MIDI-4 sets[25] were employed for C and O, and a (4s)/[2s] set[26] was used for H. A d-polarization function[25] was added to C and O, and a p-polarization function[26] was added to the active hydrogen atom that was hydride and the H atom of formate. All the transition states were ascertained by vibrational frequency calculation with the DFT/BS-I method. Energy changes were calculated with the DFT method, where geometries were taken to be the same as DFT/BS-I-optimized ones and a better basis set system (BS-II) was employed. In BS-II, a (541/541/211)[27] set was employed for Rh with the same ECPs as those in the BS-I.[24] MIDI-4 set[25] was used for P, where a d-polarization function was added.[25] For C and O, (9s 5p 1d)/[3s 2p 1d] sets[26] were used with a p-diffuse function.[26] For the active H atom, a (5s 1p)/[3s 1p] set[28] was employed. Energy changes of important elementary steps were also evaluated by the DFT/BS-II method with BLYP,[22] BP86,[29] and BPW91[30] functionals, MP4(SDQ)/BS-II, and CCSD(T)/BS-II methods. In the MP4(SDQ) and CCSD(T) calculations, core orbitals were excluded from an active space. In CCSD(T) calculations, contribution of triple excitations was taken into consideration noniteratively with the CCSD wave function.[31] The Gaussian 98 program was used in these calculations.[32]

3. Results and Discussion

3.1. Geometry and Energy Changes in the CO_2 Insertion into the Rh(III)−H Bond. Geometry changes in CO_2 insertion into the Rh(III)−H bond of $[RhH_2(PH_3)_2(L)_2]^+$ (L = PH_3 or H_2O) are shown in Figure 1. In $[RhH_2(PH_3)_4]^+$, one PH_3 ligand must dissociate from the Rh center to make a vacant site for CO_2 coordination. The resultant complex, $[RhH_2(PH_3)_3]^+$, **1a**, is 26.6 kcal/mol less stable than $[RhH_2(PH_3)_4]^+$, where the energy change calculated by the DFT/BS-II method is given hereafter without any comment. In $[RhH_2(PH_3)_2(H_2O)_2]^+$, H_2O dissociates from the Rh center to form $[RhH_2(PH_3)_2(H_2O)]^+$, **1b**, with a destabilization energy of 25.0 kcal/mol. CO_2 coordinates to **1a,b** to form precursor complexes, $[RhH_2(PH_3)_3(CO_2)]^+$, **2a**, and $[RhH_2(PH_3)_2(H_2O)(CO_2)]^+$, **2b**, with stabilization energies of 8.0 and 10.8 kcal/mol, respectively. From **2a,b**,

(17) (a) Lee, J. C., Jr.; Rheingold, A. L.; Muller, B.; Pregosin, P. S.; Crabtree, R. H. *J. Chem. Soc., Chem. Commun.* **1994**, 1021. (b) Lee, J. C., Jr.; Peris, E.; Rheingold, A. L.; Crabtree, R. H. *J. Am. Chem. Soc.* **1994**, *116*, 11014. (c) Crabtree, R. H.; Siegbahn, P. E. M.; Eisenstein, O.; Rheingold, A. L.; Koetzle, T. F. *Acc. Chem. Res.* **1996**, *29*, 348.
(18) (a) Milet, A.; Dedieu, A.; Kapteijn, G.; Koten, G. van *Inorg. Chem.* **1997**, *36*, 3223. (b) Milet, A.; Dedieu, A.; Canty, A. J. *Organometallics* **1997**, *16*, 5331.
(19) Musashi, Y.; Sakaki, S. *J. Chem. Soc., Dalton Trans.* **1998**, 577.
(20) Parr, R. G.; Yang, W. *Density-Functional Theory of Atoms and Molecules*; Oxford University Press: New York, 1989.
(21) (a) Becke, A. D. *Phys. Rev. A* **1988**, *38*, 3098. (b) Becke, A. D. *J. Chem. Phys.* **1993**, *98*, 1372. (c) Becke, A. D. *J. Chem. Phys.* **1993**, *98*, 5648.
(22) Lee, C.; Yang, W.; Parr, R. G. *Phys. Rev. B* **1988**, *37*, 785.
(23) Hay, P. J.; Wadt, W. R. *J. Chem. Phys.* **1985**, *82*, 299.
(24) Wadt, W. R.; Hay, P. J. *J. Chem. Phys.* **1985**, *82*, 284.
(25) Huzinaga, S.; Andzelm, J.; Klobukowski, M.; Radzio-Andzelm, E.; Sakai, Y.; Tatewaki, H. *Gaussian Basis Sets for Molecular Calculations*; Elsevier: Amsterdam, 1984.
(26) Dunning, T. H.; Hay, P. J. *Methods of Electronic Structure Theory*; Schaefer, H. F., Plenum: New York, 1977; p 1.
(27) Couty, M.; Hall, M. B. *J. Comput. Chem.* **1996**, *17*, 1359.
(28) Clark, T.; Chandrasekhar, J.; Spitznagel, G. W.; Schleyer, P. v. R. *J. Comput. Chem.* **1983**, *4*, 294.
(29) (a) Perdew, J. P. *Phys. Rev. B* **1986**, *33*, 8822. (b) Perdew, J. P. *Phys. Rev. B* **1986**, *34*, 7046.
(30) Perdew, J. P.; Wang, Y. In *Electronic Strucutre of Solids '91*; Ziesche, P., Eschrig, H. E., Eds.; Akademie-Verlag: Berlin, 1991.
(31) Pople, J. A.; Head-Gordon, M.; Raghavachari, K. *J. Chem. Phys.* **1987**, *87*, 5968.
(32) Frisch, M. J.; Trucks, G. W.; Schlegel, H. B.; Scuseria, G. E.; Robb, M. A.; Cheeseman, J. R.; Zakrzewski, V. G.; Montgomery, J. A.; Stratmann, R. E.; Burant, J. C.; Dapprich, S.; Millam, J. M.; Daniels, A. D.; Kudin, K. N.; Strain, M. C.; Farkas, O.; Tomasi, J.; Barone, V.; Cossi, M.; Cammi, R.; Mennucci, B.; Pomelli, C.; Adamo, C.; Clifford, S.; Ochterski, J.; Petterson, G. A.; Ayala, P. Y.; Cui, Q.; Morokuma, K.; Malick, D. K.; Rabuck, A. D.; Raghavachari, K.; Foresman, J. B.; Cioslowski, J.; Ortiz, J. V.; Stefanov, B. B.; Liu, G.; Liashenko, A.; Piskorz, P.; Komoromi, I.; Gomperts, R.; Martin, R. L.; Fox, D. J.; Keith, T.; Al-Laham, M. A.; Peng, C. Y.; Nanayakkara, A.; Gonzalez, C.; Challacombe, M.; Gill, P. M. W.; Johnson, B. G.; Chen, W.; Wong, M. W.; Andres, J. L.; Head-Gordon, M.; Replogle, E. S.; Pople, J. A. *GAUSSIAN 98 (Revision A7)*; Gaussian Inc.: Pittsburgh, PA, 1998.

CO_2 is inserted into the Rh(III)−H bond through a four-centered transition state (TS), **TS_{2a-3a}** and **TS_{2b-3b}**, to afford [RhH(η^1-OCOH)$(PH_3)_3$]$^+$, **3a**, and [RhH(η^1-OCOH)$(PH_3)_2(H_2O)$]$^+$, **3b**, respectively. The eigenvector with an imaginary frequency (293i cm^{-1} in **TS_{2a-3a}** and 74i cm^{-1} in **TS_{2b-3b}**) mainly involves Rh−H^2 bond breaking and Rh−O^1 bond formation (see Supporting Information). In **TS_{2a-3a}** and **TS_{2b-3b}**, the C−H^2, C−O^1, and Rh−O^1 distances are similar to those of the product (**3a,b**). These geometrical features clearly indicate that the formate anion and the Rh−O^1 bond are almost formed in these TS's. In **TS_{2a-3a}**, CO_2 avoids the position trans to the H ligand and approaches the H ligand, while CO_2 does not considerably change its position and the H ligand approaches CO_2 in **TS_{2b-3b}**. This is because trans-influence of the H ligand is strong but that of PH_3 is weak. Product **3a** takes a five-coordinate pseudo-square-pyramidal structure, as shown in Figure 1. The H^1 atom is at a position trans to an empty site because of the strong trans-influence of the H ligand. The Rh−H^1 bond distance (1.513 Å) is similar to those of $[RhH_2(PH_3)_4]^+$ [33] and [RhH_2-(η^5-C_5Me_5)$(SiEt_3)_2$].[34] The Rh−P^3 bond is longer than the Rh−P^1 and Rh−P^2 bonds, which indicates that the trans-influence of the η^1-OCOH ligand is stronger than that of PH_3. These geometry changes are essentially the same as those optimized previously with the MP2 method.[19] In **3b**, the Rh−H^2 distance (1.945 Å) is shorter than that of **TS_{2b-3b}** because the agostic interaction is formed between the C−H^2 bond and the Rh center. The η^1-OCOH ligand still takes a position trans to PH_3 in **3b** unlike that in **3a**, since the trans-influence of PH_3 is much weaker than that of the H ligand.

The activation barrier (E_a) and the reaction energy (ΔE) of the CO_2 insertion are defined as an energy difference between the precursor complex and the TS and that between the precursor complex and the product, respectively. In the insertion reaction of **2a**, the E_a and ΔE values were calculated to be 47.2 and 27.8 kcal/mol, respectively, with the DFT(B3LYP) method. In the insertion reaction of **2b**, the E_a and ΔE values were evaluated to be 28.4 and 27.9 kcal/mol, respectively.

E_a and ΔE values were also evaluated by the DFT method with various functionals, MP2-MP4(SDQ), and CCSD(T) methods, as shown in Table 1. Although E_a and ΔE values slightly fluctuate around the MP3 method, these values converge upon going to CCSD(T). It is noted that the DFT(B3LYP) method yields slightly smaller E_a and ΔE values than does the CCSD(T) method and that BLYP, BP86, and BPW91 functionals[35,36] provide further smaller E_a value than the B3LYP functional. Since the differences in E_a and ΔE between the DFT(B3LYP) and CCSD(T) methods are not large and the DFT(B3LYP) method yields better H−OCOH bond energy than the CCSD(T) method,[37] we adopted E_a and ΔE values calculated by the DFT(B3LYP) method in our discussion.

It is of considerable importance to clarify the reason for the higher reactivity of **2b** than that of **2a**. In the TS, the Rh−η^1-OCOH bond is almost formed. In **2a**, the Rh−η^1-OCOH bond should be formed at a position trans to the H ligand, while it is formed at a position trans to PH_3 in **2b**. Since the trans-influence of the H ligand is much stronger than that of PH_3, **TS_{2a-3a}** suffers from the trans-influence of the H ligand to a much greater extent than **TS_{2b-3b}**. As a result, CO_2 is much more easily inserted into the Rh(III)−H bond in **2b** than that in **2a**.

Our previous calculations indicated that CO_2 was inserted into the Ru(II)−H bond of $RuH_2(PH_3)_3$ with a smaller E_a value of 11.0 kcal/mol (CCSD(T) calculation).[15] Also, CO_2 was easily inserted into the Rh(I)−H bond of $RhH(PH_3)_2$ with a very small E_a value, 4.3 kcal/mol by MP2 calculation, no barrier by QCISD(T) calculation,[13a] and 1.6 kcal/mol by DFT(B3LYP) calculation.[38] From these results, it is clearly concluded that the reactivity for the CO_2 insertion is significantly different among rhodium(I), rhodium(III), and ruthenium(II) complexes.

Table 1. Activation Barrier (E_a) and Reaction Energy (ΔE) of CO_2 Insertion, Three-Centered H−OCOH Reductive Elimination, **3a** → **3c** Isomerization, Five-Centered H−OCOH Reductive Elimination (**3a** → **4a**), and **3d** → **3e** Isomerization (kcal/mol)[a]

	CO_2 insertion				three-centered H–OCOH reductive elimination (**3a** → **4a**)	
	2a → **3a**		**2b** → **3b**			
	E_a	ΔE	E_a	ΔE	E_a	ΔE
MP2	55.7	37.4	33.9	36.6	21.3	−29.8
MP3	54.2	32.4	35.7	34.8	24.4	−37.0
MP4(DQ)	56.2	36.4	32.7	37.5	23.4	−35.1
MP4(SDQ)	53.8	34.8	35.8	34.8	22.2	−34.9
CCSD	52.7	32.8	34.3	34.8	23.7	−35.7
CCSD(T)	50.9	32.1	33.1	32.4	22.2	−33.8
DFT(B3LYP)	47.2	27.8	28.4	27.9	19.6	−34.8
DFT(BLYP)	42.3	26.1	26.1	24.3	17.1	−29.2
DFT(BP86)	41.0	25.6	25.4	22.1	17.4	−29.2
DFT(BPW91)	41.8	26.3	26.1	22.8	17.5	−29.3

	isomerization **3a** → **3c**	five-centered H–OCOH reductive elimination (**3a** → **4a**)	isomerization **3d** → **3e**	
	E_a	ΔE	E_a	ΔE
MP2	2.8	−29.8	1.7	−10.6
MP3	−0.5	−37.0	0.7	−10.3
MP4(DQ)	0.4	−35.1	0.7	−10.5
MP4(SDQ)	1.5	−34.9	1.6	−10.1
CCSD	0.5	−35.7	1.3	−10.2
CCSD(T)	1.3	−33.8	1.8	−10.1
DFT(B3LYP)	2.7	−34.8	2.8	−9.1
DFT(BLYP)	3.6	−29.2	4.3	−7.9
DFT(BP86)	4.8	−29.2	4.6	−8.4
DFT(BPW91)	5.0	−29.3	4.7	−8.3

[a] BS-II was used.

3.2. Geometry Changes in the Reductive Elimination of Formic Acid. Though the CO_2 insertion in **2a** needs a much larger activation barrier than that in **2b** (vide supra), we take into account of the possibility that successive elementary steps starting from **3b** occur with larger activation barriers than those steps starting from **3a**. Thus, we investigated the H−OCOH reductive elimination in both **3a** and **3b**. Three-centered reductive elimination of **3a** proceeds through the transition state **TS_{3a-4a}**, in which the H^1 atom considerably moves toward the O^1 atom but the Rh−H^1 distance (1.572 Å) little lengthens, as shown in Figure 2. This course is called path A, herewith. The O^1−H^1 distance (1.542 Å) is much longer than the usual O−H bond distance but significantly shorter than that of **5c** (see Figure

(33) Macgregor, S. A.; Eisenstein, O.; Whittlesey, M. K.; Perutz, R. N. *J. Chem. Soc., Dalton Trans.* **1998**, 291.
(34) Fernadez, M.-J.; Bailey, P. M.; Bentz, P. O.; Ricci, J. S.; Koetzle, T. F.; Maitlis, P. M. *J. Am. Chem. Soc.* **1984**, *106*, 5458.
(35) Barden, C. J.; Rienstra-Kiracofe, J. C.; Schaefer, H. F., III. *J. Chem. Phys.* **2000**, *113*, 690.
(36) García-Sosa, A. T.; Castro, M. *Int. J. Quantum Chem.* **2000**, *80*, 307.
(37) (a) The H−OCOH bond energy is calculated to be 128.5, 125.8, 126.0, 124.1, 116.6, 114.8, and 112.3 kcal/mol, by MP2, MP3, MP4(SDQ), CCSD(T), DFT(B3LYP), and G2MP2 methods,[37b] respectively. (b) Curtiss, L. A.; Raghavachari, K.; Trucks, G. W.; Pople, J. A. *J. Chem. Phys.* **1993**, *98*, 1293.
(38) The DFT(B3LYP)/BS-II method was used, where the geometries were reoptimized here with the DFT(B3LYP)/BS-I method.

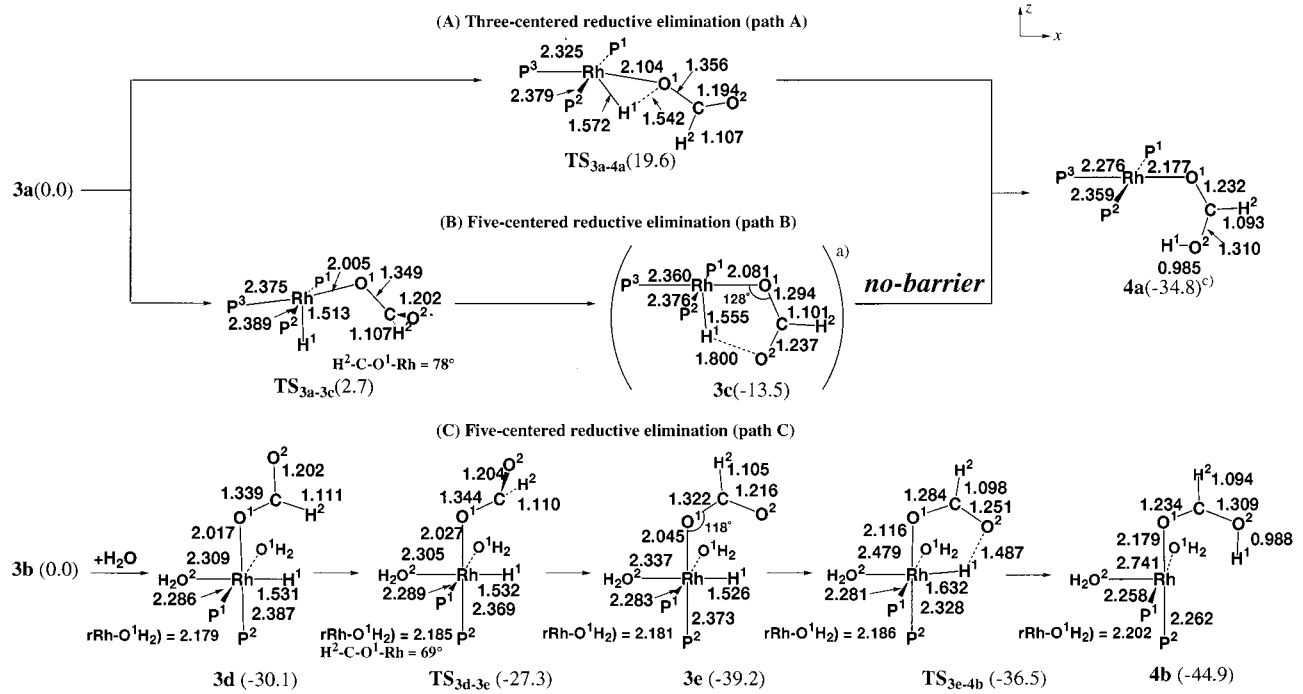

Figure 2. Geometry changes in the reductive elimination of formic acid from $[RhH(\eta^1\text{-}OCOH)(PH_3)_2(L)_n]^+$ (L = PH_3 or H_2O; n = 1, 2). Bond distances are in Å, and bond angles are in deg. (a) This is not a local minimum. This structure is optimized with the O^2-H^1 distance fixed to 1.8 Å. (b) In parentheses are the energy differences from either **3a** (L = PH_3) or **3b** (L = H_2O) (kcal/mol unit; the DFT(B3LYP)/BS-II//DFT(B3LYP)/BS-I calculation). (c) Product **4a** is a product of both paths A and B. Since path B needs a lower activation barrier than path A, we assign numbers to O atoms, consistent with $\mathbf{TS_{3a-3c}}$ (path B). As a result, this assignment becomes inconsistent with $\mathbf{TS_{3a-4a}}$.

4). The $Rh-O^1$ bond (2.104 Å) is only 0.108 Å longer than that of **3a**. These features suggest that although the RhH-(η^1-OCOH)$(PH_3)_3$ moiety considerably distorts, both Rh−H and $Rh-O^1$ bonds are not broken yet and the O−H bonding interaction is still weak; in other words, the geometry of RhH-(η^1-OCOH)$(PH_3)_3$ moiety considerably distorts in $\mathbf{TS_{3a-4a}}$ without suffcient O−H bond formation, which leads to the large E_a value (vide infra).

$\mathbf{TS_{3a-4a}}$ exhibits only one imaginary frequency (971i cm^{-1}), of which eigenvector mainly involves the approach of H^1 to O^1 (see Supporting Information). The geometry optimization starting from $\mathbf{TS_{3a-4a}}$ directly leads to $[Rh(PH_3)_3(HCOOH)]^+$, **4a** (see Figure 2). Complex **4a** takes a four-coordinate planar structure because of a d^8 electron configuration of Rh(I). In **4a**, the $C-O^1$ distance (1.232 Å) is somewhat longer than the C=O double bond of free formic acid (r(C−O) = 1.203 Å), probably because the O atom coordinates with the Rh(I) center. Elimination of HCOOH from the Rh center gives rise to a considerably large destabilization energy of 26.5 kcal/mol. This is because formic acid strongly coordinates with the Rh center. Actually, the $Rh-O^1$ distance (2.177 Å) is similar to the usual coordinate bond distance.

Since the five-centered reductive elimination can take place when the O^2 atom is in the same side as the H^1 atom, as shown in Chart 1B, **3a** must isomerize to **3c** (see Figure 2). This isomerization would occur through the rotation of the OCH moiety about the $C-O^1$ bond. In the transition state $\mathbf{TS_{3a-3c}}$ (141i cm^{-1}), the dihedral angle between O−C−O and Rh−O−C planes is about 80°, as shown in Figure 2, whereas the geometry of the other moiety little changes. These features suggest that the η^1-OCOH moiety easily rotates without significant geometry change of the other moiety. Consistent with this suggestion, the activation barrier is very small (E_a = 2.7 kcal/mol). Then, we tried to optimize the product of isomerization, **3c**. However, the optimization of **3c** spontaneously led to $[Rh(PH_3)_3(HCOOH)]^+$, **4a** (see Figure 2 for **4a**). This means that $\mathbf{TS_{3a-3c}}$ is only one transition state between **3a** and **4a**. To ascertain if the reductive elimination can take place from **3c** with no barrier, we investigated the geometry and energy changes from **3c** to **4a**, taking the O^2-H^1 distance as an approximate reaction coordinate, where the geometry of **3c** was optimized under assumption that the O^2-H^1 distance was arbitrarily fixed to be 1.80 Å. As the O^2-H^1 distance decreases from 1.80 Å, the $Rh-O^1$ bond gradually lengthens, while the O^1 and O^2 atoms move little (see Supporting Information). Simultaneously, the $C-O^1$ distance shortens and the $C-O^2$ distance lengthens, and the total energy monotonically decreases without any barrier. These results clearly indicate that the five-centered reductive elimination proceeds with no barrier after isomerization of **3a** to **3c**. This reaction course from **3a** to **4a** is called path B hereafter.

Considering that the five-centered reductive elimination much more easily occurs than the three-centered one in **3a**, we investigated only the five-centered reductive elimination starting from $[RhH(\eta^1\text{-}OCOH)(PH_3)_2(H_2O)]^+$, **3b**. This reaction course is called path C. H_2O easily coordinates to **3b** to yield [RhH-(η^1-OCOH)$(PH_3)_2(H_2O)_2]^+$, **3d**, with a stabilization energy of 30.1 kcal/mol. Since the O^2 atom must take a position in the same side as the H^1 ligand in the five-centered reductive elimination, isomerization of **3d** to **3e** necessarily occurs, as shown in Figure 2. This isomerization proceeds through the transition state $\mathbf{TS_{3d-3e}}$ (144i cm^{-1}), in which the dihedral angle between O−C−O and Rh−O−C planes is 69°, similar to the geometry of $\mathbf{TS_{3a-3c}}$. The five-centered reductive elimination

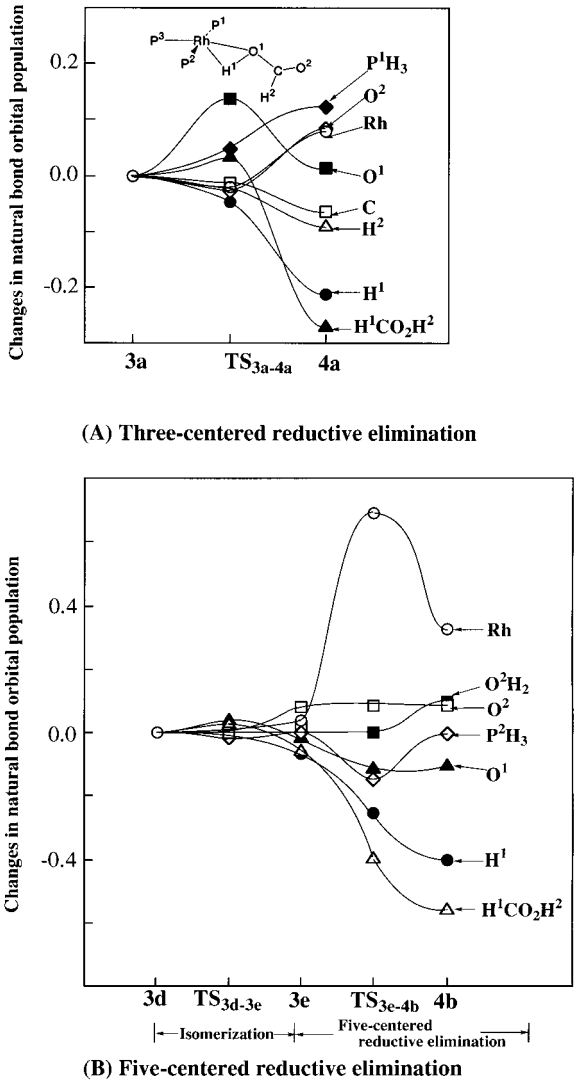

Figure 3. Population changes in the reductive elimination of formic acid from $[RhH(\eta^1\text{-OCOH})(PH_3)_2(L)_n]^+$ (L = PH_3 or H_2O; $n = 1, 2$). The natural bond orbital population[39] is determined with the DFT(B3LYP)/BS-II//DFT-(B3LYP)/BS-I calculation. A positive value represents an increase in population relative to either **3a** or **3d**.

of **3e** occurs through $\mathbf{TS_{3e-4b}}$ (567i cm^{-1}), to yield $[Rh(PH_3)_2(H_2O)_2(HCOOH)]^+$, **4b**. In $\mathbf{TS_{3e-4b}}$, the Rh−H^1 bond lengthens a little by 0.106 Å and the O^2−H^1 distance (1.487 Å) is much longer than that of **4b**. These features indicate that the Rh−H bond is not broken yet and the O−H bonding interaction is still weak in $\mathbf{TS_{3e-4b}}$ and that this TS is reactant-like. In **4b**, the η^1-OCOH moiety resembles well that of **4a**.

3.3. Energy and Population Changes in the Reductive Elimination of Formic Acid. The activation barrier (E_a) of the three-centered reductive elimination, which is defined as an energy difference between **3a** and $\mathbf{TS_{3a-4a}}$ ($E_a = E_t(\mathbf{TS_{3a-4a}}) - E_t(\mathbf{3a})$), is calculated to be 19.6 kcal/mol with the DFT-(B3LYP) method and about 17 kcal/mol with the DFT(BLYP), DFT(BP86), and DFT(BPW91) methods. As listed in Tables 1 and 2, both MP4(SDQ) and CCSD(T) methods provide the activation barrier of 22.2 kcal/mol, which is slightly larger than that calculated with the DFT(B3LYP) method. The activation barrier of the **3a** → **3c** isomerization, which is defined as an energy difference between **3a** and $\mathbf{TS_{3a-3c}}$, is calculated to be very small with all the computational methods, as shown in

Table 2. Activation Barrier (E_a) and Reaction Energy (ΔE) of Five-Centered H−OCOH Reductive Elimination (**3e** → **4b**), Four-Centered σ-Bond Metathesis, **5a** → **5c** Isomerization, and Six-Centered σ-Bond Metathesis (**5c** → **6c** and **5b** → **6b**) (kcal/mol)[a]

	five-centered H–OCOH reductive elimination (**3e** → **4b**)		four-centered σ-bond metathesis (**5a** → **6a**)	
	E_a	ΔE	E_a	ΔE
MP2	3.4	1.0	24.2	−5.6
MP3	7.8	−4.5	26.0	−5.1
MP4(DQ)	6.5	−3.6	25.2	−7.1
MP4(SDQ)	5.2	−3.8	25.7	−5.1
CCSD	6.8	−4.2	26.1	−4.6
CCSD(T)	5.3	−2.5	25.8	−3.5
DFT(B3LYP)	2.7	−5.7	21.9	−3.5
DFT(BLYP)	1.7	−1.7	21.8	0.9
DFT(BP86)	0.7	−0.6	18.9	−2.3
DFT(BPW91)	0.5	−1.7	19.3	−2.3

	isomerization **5a** → **5c**		six-centered σ-bond metathesis (**5c** → **6c**)		six-centered σ-bond metathesis (**5b** → **6b**)	
	E_a	ΔE	E_a	ΔE	E_a[b]	ΔE
MP2	12.5	−14.1	1.3	−4.6	4.8	−41.5
MP3	10.2	−13.1	2.5	−5.3	3.6	−44.5
MP4(DQ)	10.6	−13.3	2.4	−5.9	3.7	−42.5
MP4(SDQ)	11.6	−13.0	2.1	−4.9	4.6	−42.9
CCSD	10.8	−12.8	2.5	−4.6	4.1	−40.8
CCSD(T)	12.0	−13.0	1.9	−4.2	4.8	−33.7
DFT(B3LYP)	10.2	−13.5	0.4	−4.6	5.9	−39.1
DFT(BLYP)	10.4	−12.1	0.2	−1.8	7.4	−33.7
DFT(BP86)	10.8	−14.1	−1.2	−4.3	8.0	−34.6
DFT(BPW91)	10.7	−13.6	−1.1	−4.4	7.9	−34.9

[a] BS-II was used. [b]The activation barrier of the **5b** → **5d** isomerization.

Table 1. From **3c**, the five-centered reductive elimination occurs with no barrier (vide supra) and its reaction energy ($\Delta E = E_t(\mathbf{4a}) - E_t(\mathbf{3a})$) is significantly negative. Since the activation barrier of the three-centered reductive elimination is much larger than those of the **3a** → **3c** isomerization and the five-centered reductive elimination of **3c** in all the computational methods, it should be concluded that the three-centered reductive elimination of formic acid much less easily occurs than the isomerization followed by five-centered reductive elimination.

The activation barrier of the **3d** → **3e** isomerization is calculated to be 2.8 kcal/mol. After the isomerization, the five-centered reductive elimination of **3e** easily occurs with a very small activation barrier (2.7 kcal/mol), as shown in Table 2. These results show that formic acid is easily formed from **3d** through isomerization and five-centered H−OCOH reductive elimination.

It is worthwhile to investigate electron population changes in these three-centered and five-centered reductive eliminations, where NBO analysis[39] was adopted to evaluate electron population. As shown in Figure 3, H^1 atomic population decreases in both reductive eliminations. This population decrease clearly indicates that the H^1 atom changes into proton (H^+) in both reductive eliminations. In the three-centered reductive elimination, O^1 atomic population increases at $\mathbf{TS_{3a-4a}}$ but then decreases, while Rh atomic population slightly decreases at $\mathbf{TS_{3a-4a}}$ and then somewhat increases in the product (Figure 3A). In the five-centered reductive elimination of **3d** to **4b**, H^1 atomic population smoothly decreases and Rh atomic population smoothly increases, while O^1 and O^2 atomic populations little

(39) Reed, A. E.; Curtiss, L. A.; Weinhold, F. *Chem. Rev.* **1988**, *88*, 899 and references therein.

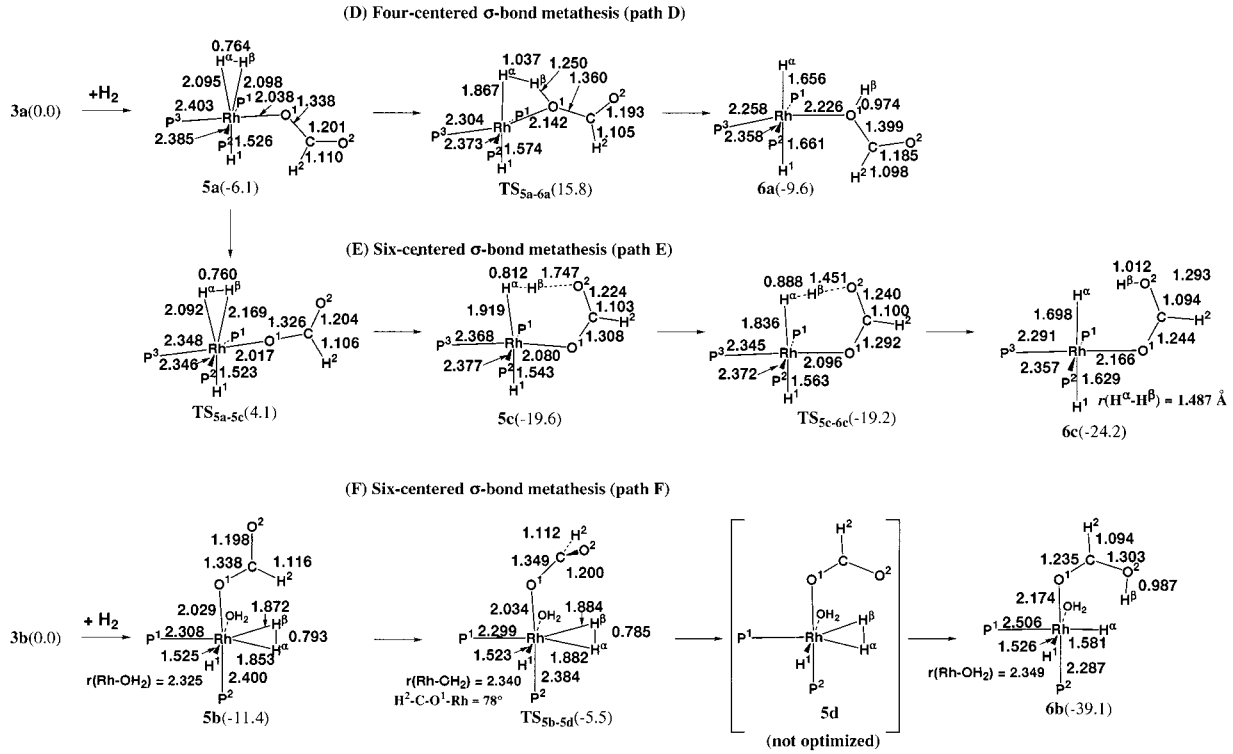

Figure 4. Geometry changes in the σ-bond metathesis of $[RhH(\eta^1\text{-}OCOH)(PH_3)_2(L)]^+$ with H_2 (L = PH_3 or H_2O). Bond distances are in Å. In parentheses are the energy difference from either **3a** (L = PH_3) or **3b** (L = H_2O) (kcal/mol unit; the DFT(B3LYP)/BS-II//DFT(B3LYP)/BS-I calculation).

Chart 2

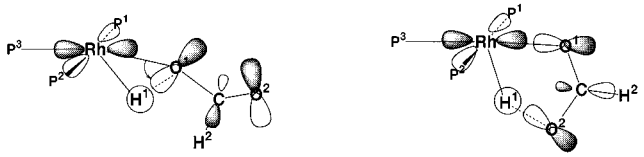

change, as shown in Figure 3B. In the reductive elimination of **3c** to **4a**, electron populations change in almost the same manner as those of reductive elimination of **3d** to **4b** (see Supporting Information). These results show that electron populations smoothly change in the five-centered reductive elimination but not smoothly in the three-centered reductive elimination. This difference between three-centered and five-centered reductive eliminations would be related to the reason that the five-centered reductive elimination occurs more easily than the three-centered reductive elimination, as follows: In the three-centered reductive elimination, the O^1 p orbital of the HOMO (ϕ_{HOMO}) of η^1-OCOH[40] must change its direction toward H^1 to form a new O−H bond, as shown in Chart 2. This direction change suppresses the charge transfer from the η^1-formate anion to the Rh center, which leads to the decrease in Rh atomic population and the increase in O^1 atomic population at $\mathbf{TS_{3a-4a}}$. At the same time, this direction change weakens the Rh−O^1 bond. Thus, the three-centered reductive elimination needs a considerably large E_a value. In the five-centered reductive elimination, on the other hand, the O^2 p orbital of ϕ_{HOMO} expands well toward the H^1 atom in **3c**, as shown in Chart 2. Also, the O^1 p orbital of ϕ_{HOMO} can keep the Rh−O^1 bonding interaction during the reaction. Because of these features, electron populations smoothly change and the O^2−H^1 bond is smoothly formed without considerable weakening of the Rh−O^1 bond. Thus, the five-centered H−OCOH reductive elimination easily takes place with no barrier or very small barrier.

3.4. Geometry Changes in σ-Bond Metathesis of $[RhH(\eta^1\text{-}OCOH)(PH_3)_2(L)]^+$ (L = PH_3 or H_2O) with H_2. Geometry changes in four-centered and six-centered σ-bond metatheses are shown in Figure 4. The first step of these σ-bond metatheses is coordination of H_2 to **3a,b**. This coordination easily takes place to yield $[RhH(\eta^1\text{-}OCOH)(PH_3)_3(H_2)]^+$, **5a**, and $[RhH(\eta^1\text{-}OCOH)(PH_3)_2(H_2O)(H_2)]^+$, **5b**, since **3a,b** have an empty coordination site. The H_2 coordination energy of **5a** is calculated to be 6.1, 8.4, and 8.8 kcal/mol by the DFT(B3LYP), MP4(SDQ), and CCSD(T) methods, respectively, and that of **5b** is calculated to be 10.4, 13.0, and 12.6 kcal/mol by the DFT(B3LYP), MP4(SDQ), and CCSD(T) methods, respectively. These coordination energies are similar to that (7.1 kcal/mol) calculated for $Rh(\eta^1\text{-}OCOH)(PH_3)_2(H_2)$ (see below). In **5a,b**, the H^α−H^β bond (0.764 and 0.793 Å, respectively) is slightly longer than that of free hydrogen molecule (see Figure 4 for H^α and H^β) but significantly shorter than that of $RhCl(PH_3)_2(H_2)$ (0.863 Å) in which the H_2 coordination energy is 20.1 kcal/mol by the Hartree−Fock calculation.[41] The Rh−H^α and Rh−H^β distances (about 2.1 and 1.9 Å) are somewhat longer than those of $Rh(\eta^1\text{-}OCOH)(PH_3)_2(H_2)$ (about 1.8 Å)[13a] and much longer than those of $RhCl(PH_3)_2(H_2)$ (1.65 Å).[41] These results show that the coordinate bond of H_2 in **5a,b** is much weaker than that of $RhCl(PH_3)_2(H_2)$ and the H^α−H^β bond is much less activated by the coordination with the Rh center than

(40) HOMO of free $OCOH^-$ is on the O−C−O plane and involves the antibonding overlap with the C p orbital. The next HOMO is also on the O−C−O plane but does not involve any interaction with the C atom; in other words, this is nonbonding orbital. Below the next HOMO, there is a nonbonding π ($n\pi$) orbital which is perpendicular to the O−C−O plane and the Rh−O bond. The HOMO mainly participates in the metal−formate bonding interaction, as shown in Chart 2.

(41) Daniel, D.; Koga, N.; Han, J.; Fu, X. Y.; Morokuma, K. *J. Am. Chem. Soc.* **1988**, *110*, 3773.

Chart 3

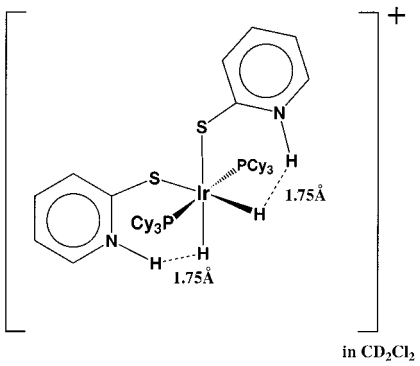

that of $RhCl(PH_3)_2(H_2)$. The $Rh-O^1$ distances (2.038 and 2.029 Å) of **5a,b** are slightly longer than those of **3a,b**, probably because **5a,b** possess one more ligand than **3a,b**.

From **5a**, the σ-bond metathesis proceeds through the four-centered transition state $\mathbf{TS_{5a-6a}}$, to afford $[RhH_2(PH_3)_3(HCOOH)]^+$, **6a**, as shown in Figure 4. This reaction course is called path D hereafter. Only one imaginary frequency (1540i cm^{-1}) is observed in $\mathbf{TS_{5a-6a}}$, of which eigenvector mainly involves approach of H^α to Rh and that of H^β to O^1. In this transition state, the $H^\alpha-H^\beta$ distance is much longer than that of **5a** by 0.273 Å and the $Rh-O^1$ and $C-O^1$ distances are intermediate between those of **5a** and **6a**, while the O^1-H^β distance (1.250 Å) is considerably longer than the usual O−H bond, as shown in Figure 4. These features indicate that the H−H bond becomes considerably weak but the O−H bond is still weak in this $\mathbf{TS_{5a-6a}}$. The $Rh-O^1$ bond (2.226 Å) of **6a** is much longer than those of **4a,b**. This is because the O atom in the C═O double bond coordinates with the Rh center in **4a,b** but the O atom in the C−O−H single bond coordinates with the Rh center in **6a**. Actually, the O p orbital of the C═O double bond in the HOMO (ϕ_{HOMO}) of formic acid is at a higher energy than the O p orbital (ϕ_{HOMO-2}) in the C−O−H bond of formic acid; the former ϕ_{HOMO} is at −8.40 eV (−12.97 eV), and the latter ϕ_{HOMO-2} is −11.53 eV (−16.52 eV), where in parentheses are orbital energies by Hartree−Fock/BS-II calculation and out of parentheses are energies of the Kohn−Sham orbital by DFT-(B3LYP)/BS-II calculation.

The six-centered σ-bond metathesis can occur, when the dihydrogen molecule takes a position in the same side of the O^2 atom of η^1-OCOH. Thus, **5a** must isomerize to **5c**, as shown in Figure 4. In the transition state $\mathbf{TS_{5a-5c}}$ (275i cm^{-1}) of this isomerization, the $Rh-P^3$ and $Rh-H^\beta$ bonds slightly lengthen by 0.054 and 0.071 Å, respectively, while the other bond distances change little. Several differences are observed between **5a** and **5c**, as follows: (1) The $H^\alpha-H^\beta$ distance (0.812 Å) of **5c** is significantly longer than that (0.764 Å) of **5a**, which shows that the H_2 moiety is more activated in **5c** than in **5a**. (2) The $H^\beta\cdots O^2$ distance (1.747 Å) is rather short in **5c**, while the O^2 atom is much distant from the H^β atom in **5a**. (3) H^α and H^β atomic charges are $+0.017e$ and $+0.204e$, respectively, in **5c**, while they are $+0.067e$ and $+0.137e$, respectively, in **5a**. These electron populations indicate that the H_2 moiety in **5c** is more polarized than that in **5a**. This polarization is induced by the electrostatic interaction with the O^2 atom of formate. Morris et al. experimentally reported the similar six-centered interaction (see Chart 3) in $[Ir\{H(\eta^1\text{-}SC_5H_4NH)\}_2(PCy_3)_2]BF_4$.[16] Because of this intramolecular interaction, **5c** is much more stable than **5a** by 13.5 kcal/mol, and therefore, the isomerization is exothermic. If one starts from **5c**, the σ-bond metathesis takes place through a six-centered transition state $\mathbf{TS_{5c-6c}}$. Only one imaginary frequency of 451i cm^{-1} is observed in $\mathbf{TS_{5c-6c}}$, of which eigenvector mainly involves approach of H^α to Rh and that of H^β to O^2. In this transition state, the O^2-H^β distance (1.451 Å) becomes shorter than that of **5c** by 0.296 Å. Geometry of the other moiety moderately changes; for instance, the $H^\alpha-H^\beta$, $Rh-O^1$, and $Rh-H^1$ distances lengthen by only 0.076, 0.016, and 0.020 Å, respectively, and the $Rh-H^\alpha$ distance (1.836 Å) shortens by 0.083 Å. These features indicate that H^α and H^β can approach Rh and O^2, respectively, without considerably large geometry changes of the other moiety. This leads to the very small activation barrier (0.4 kcal/mol). Lee et al. reported the similar feature in the reaction between $[IrH_2\{(C_9H_6N)\text{-}N{=}C(OH)Me\}(PPh_3)_2]^+$ and H_2.[17] Product **6c** takes a six-coordinate pseudooctahedral structure because **6c** is a Rh(III) complex with a d^6 electron configuration. This reaction course from **5a** to **6c** is called path E hereafter.

Since the six-centered σ-bond metathesis of **5c** occurs much more easily than the four-centered σ-bond metathesis of **5a**, only the six-centered σ-bond metathesis was investigated in **5b**. Since dihydrogen molecule needs to take a position in the same side of the O^2 atom of η^1-OCOH to induce the six-centered σ-bond metathesis, **5b** must isomerize to **5d**, as shown in Figure 4. This isomerization takes place through the transition state $\mathbf{TS_{5b-5d}}$, in which a dihedral angle between $C-H^2-O^2$ and the $Rh-O^1-C$ planes is about 80° and the geometries of the other moiety moderately changes. Only one imaginary frequency of 192i cm^{-1} is observed in $\mathbf{TS_{5b-5d}}$, of which eigenvector mainly involves the rotation of the CH^2O^2 moiety about the $C-O^1$ bond. After the TS, only **6b** was obtained by the geometry optimization. This result shows that the six-centered σ-bond metathesis of **5d** proceeds with no barrier. The reaction course **3b** to **6b** is called path F, herewith.

At the end of this subsection, we will mention unfavorable features of the σ-bond metathesis of **5c** (path E), as follows: The product **6c** produced by this σ-bond metathesis is not stable very much, since two hydride ligands take positions trans to each other in **6c**. Actually, the Rh−H distances of **6c** are much longer than that of **3a**. Because of this unfavorable situation of **6c**, this σ-bond metathesis of **5c** to **6c** is only slightly exothermic, as will be discussed below. However, the unfavorable features disappear, if two hydride ligands take positions cis to each other. Thus, we examined here the σ-bond metathesis of **5e**, which yields a more stable product **6f** in which two hydride ligands are at positions cis to each other (see **6f** in Figure 5). The isomerization of **5a** to **5e** proceeds through substitution of $H^\alpha-H^\beta$ for $H^\gamma-H^\beta$ with a considerably large E_a value of 19.1 kcal/mol, as shown in Figure 5. In the transition state $\mathbf{TS_{5a-5e}}$, the $H^\alpha-H^\beta$ moiety is much distant from Rh, which clearly indicates that the $H^\alpha-H^\beta$ moiety does not interact suffciently with the Rh center in $\mathbf{TS_{5a-5e}}$. The eigenvector with an imaginary frequency (258i cm^{-1}) mainly involves approach of $H^\gamma-H^\delta$ to Rh (see Supporting Information). From these features, it is reasonably concluded that this reaction is characterized to be dissociative substitution. In **5e**, the $H^\gamma-H^\delta$ bond distance (0.821 Å) is much longer, the $Rh-H^\gamma$ and $Rh-H^\delta$ distances are much shorter, and the $Rh-O^1$ and $Rh-H^1$ bonds are longer

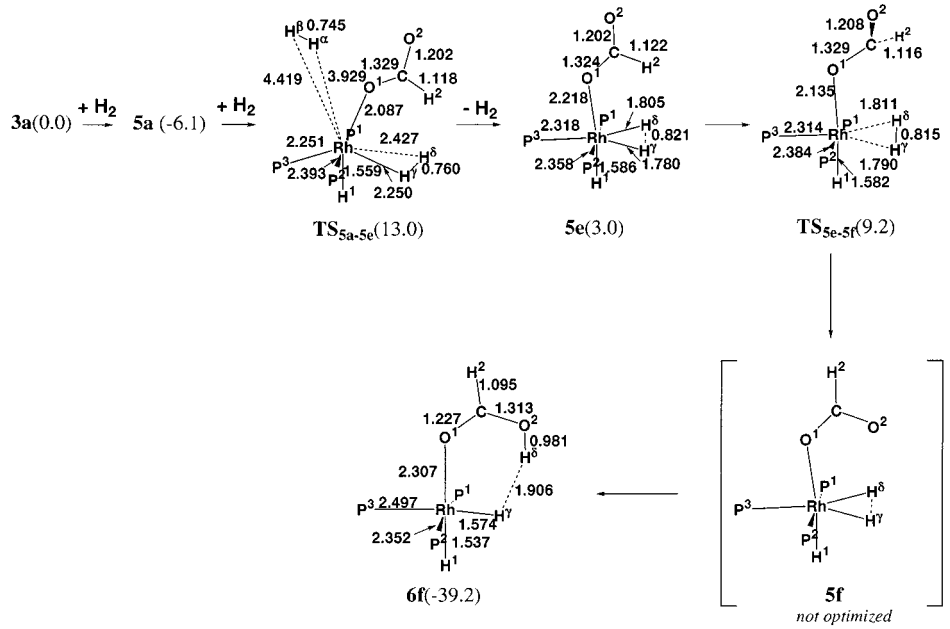

Figure 5. Geometry changes in the **5a** → **5e** isomerization followed by the σ-bond metathesis of $[RhH(\eta^1\text{-}OCOH)(PH_3)_3]^+$ with H_2. Bond distances are in Å. In parentheses are the energy differences from **3a** (kcal/mol unit; the DFT(B3LYP)/BSII//DFT(B3LYP)/BS-I calculation).

than those of **5a**. These features suggest that H_2 more strongly coordinates but η^1-OCOH less strongly coordinates with the Rh center than those in **5a**. This is because the H^1 ligand possesses strong trans-influence, as follows: The H^1 ligand weakens the coordinate bond of H_2 in **5a** but weakens the coordinate bond of η^1-OCOH in **5e**. To induce the six-centered σ-bond metathesis, **5e** must isomerize to **5f** through $\mathbf{TS_{5e-5f}}$ (129i cm^{-1}) (Figure 5). In $\mathbf{TS_{5e-5f}}$, a dihedral angle between $C-O^2-H^2$ and $Rh-O^1-C$ planes increases to 70°, while the other moiety moderately changes. Neither six-centered transition state like $\mathbf{TS_{5c-6c}}$ nor four-centered transition state like $\mathbf{TS_{5a-6a}}$ was found after $\mathbf{TS_{5e-5f}}$, and the geometry optimization starting from $\mathbf{TS_{5e-5f}}$ directly led to **6f**. In **6f**, the $Rh-O^1$ and $Rh-P^3$ bonds (2.307 and 2.497 Å, respectively) are much longer than the usual Rh−O and Rh−P bonds, respectively, because of the strong trans-influence of the H^1 ligand. Since two hydride ligands take positions cis to each other in **6f** unlike **6a,c**, **6f** is much more stable than **6a,c**. Consequently, this σ-bond metathesis is substantially exothermic ($\Delta E = E_t(\mathbf{4a}) - E_t(\mathbf{3c}) = -42.2$ kcal/mol). However, the **5a** → **5e** isomerization needs a considerably larger E_a value (19.1 kcal/mol) than those of the other six-centered σ-bond metatheses and the five-centered reductive eliminations (vide supra). Thus, we excluded this reaction course and omitted further discussion about it.

3.5. Energy and Population Changes in σ-Bond Metathesis of $[RhH(\eta^1\text{-}OCOH)(PH_3)_2(L)]^+$ (L = PH_3 or H_2O) with H_2. The activation barrier (E_a) is defined as an energy difference between transition state and intermediate just before the transition state; for instance, $E_a = E_t(\mathbf{TS_{5a-6a}}) - E_t(\mathbf{5a})$ in path D and $E_a = E_t(\mathbf{TS_{5c-6c}}) - E_t(\mathbf{5c})$ in path E (see above and Figure 4 for paths D−F). The reaction energy (ΔE) is an energy difference between the rhodium hydride formate complex, $[RhH(\eta^1\text{-}OCOH)(PH_3)_2(L)(H_2)]^+$, and the product; for instance, $\Delta E = E_t(\mathbf{6a}) - E_t(\mathbf{5a})$ in path D and $\Delta E = E_t(\mathbf{6c}) - E_t(\mathbf{5c})$ in path E. The E_a value of path D was calculated to be 21.9 kcal/mol with the DFT(B3LYP)/BS-II method. In path E, the E_a value for the six-centered σ-bond metathesis is only 0.4 kcal/mol, while the E_a value for the **5a** → **5c** isomerization is 10.2 kcal/mol. From these results, it should be concluded that path E is more favorable than path D. However, path E is much less favorable than path B which involves the five-centered reductive elimination (see Figure 2), since the **3a** → **3c** isomerization (E_a = 2.7 kcal/mol) in path B occurs with a smaller E_a value than that of the **5a** → **5c** isomerization in path E. In path F, the **5b** → **5d** isomerization takes place with a moderate E_a value of 5.9 kcal/mol, and then the six-centered σ-bond metathesis occurs with no barrier. This reaction is significantly exothermic (ΔE = −27.7 kcal/mol). Though path F is as favorable as path E, it is clearly concluded that path F is less favorable than path B, since the **5b** → **5d** isomerization of path F needs a larger E_a value than the **3a** → **3c** isomerization of path B. Although MP4(SDQ) and CCSD(T) methods provide slightly larger E_a values for the σ-bond metathesis than the DFT method, as shown in Table 2, all the computational methods indicate that the **5b** → **5d** isomerization occurs with a larger E_a value than the **3a** → **3c** isomerization. Thus, the conclusion presented here is reliable.

Why does the four-centered σ-bond metathesis (path D) need the considerably large E_a value? To clarify the reason, we calculated deformation energies of H_2 and $RhH(\eta^1\text{-}OCOH)(PH_3)_3$ moieties, where the deformation energy of an A moiety is defined as a destabilization energy that is necessary to deform only the A moiety from its equilibrium geometry to the distorted one taken in the transition state. In $\mathbf{TS_{5a-6a}}$ of the four-centered σ-bond metathesis, the deformation energy of the $RhH(\eta^1\text{-}OCOH)(PH_3)_3$ moiety is 5.5 kcal/mol and that of the H_2 moiety is 20.7 kcal/mol. In $\mathbf{TS_{5c-6c}}$ of the six-centered σ-bond metathesis, on the other hand, the deformation energies of these moieties are only 4.8 and 0.4 kcal/mol, respectively. It should be noted that the deformation energy of the H_2 moiety is much larger in the four-centered σ-bond metathesis than that in the six-centered one. This large deformation energy of the H_2 moiety comes from the considerably long H−H distance in the four-centered transition state; in other words, the H^β atom considerably moves toward the O^1 atom of formate. This is because the

Chart 4

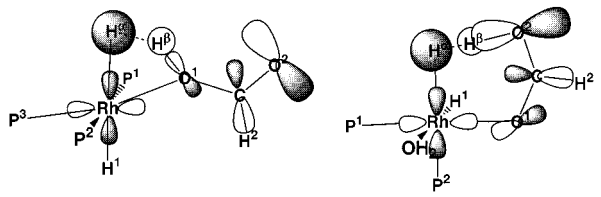

(A) Four-Centered σ-Bond Metathesis **(B) Six-Centered σ-Bond Metathesis**

O^1 p orbital of the ϕ_{HOMO}[40] of η^1-OCOH does not expand well toward the H^β atom, as shown in Chart 4A. Actually, the O^1-H^β bond distance (1.250 Å) is much longer than that in the product **6a**, whereas the $H^\alpha-H^\beta$ bond considerably lengthens in $\mathbf{TS_{5a-6a}}$. On the other hand, the $Rh-H^\alpha$ bond distance of $\mathbf{TS_{5a-6a}}$ is 0.2 Å longer than of **6a**, showing that the $Rh-H^\alpha$ bond has not been suffciently formed in $\mathbf{TS_{5a-6a}}$ despite the long $H^\alpha-H^\beta$ distance (see Figure 4). This strained geometry leads to the large E_a value of the four-centered σ-bond metathesis.

Also, population changes in the four-centered σ-bond metathesis reflect in the diffculty of this reaction. As shown in Figure 6, H^β atomic population considerably decreases in both four-centered and six-centered σ-bond metatheses. However, these two σ-bond metatheses exhibit significant differences in O^1 and H^α atomic populations. In path D including the four-centered σ-bond metathesis, O^1 and H^α atomic populations somewhat increase at $\mathbf{TS_{5a-6a}}$ but then decrease at **6a** (see Figure 6A). This unusual electron redistribution would arise from the fact that the geometry change does not occur smoothly. In path F including the six-centered σ-bond metathesis of **5b**, on the other hand, the electron populations smoothly change, as shown in Figure 6B. This is because the H^β atom takes a favorable position to form a bonding interaction with the O^2 p orbital of ϕ_{HOMO}[40] in **5d**, as shown in Chart 4B. Thus, the six-centered σ-bond metathesis easily occurs but the four-centered σ-bond metathesis needs a considerably large activation barrier. Though the population changes in path E including the six-centered σ-bond metathesis occur similarly to those of path F (see Supporting Information), moderate differences are observed, as follows: the Rh atomic population increases, but the electron population of $H^\beta CO_2H^2$ decreases to a much greater extent than those of path E. These differences are interpreted in terms that the H_2O ligand is less electron donating than PH_3 and thereby the Rh center can accept electrons from the η^1-OCOH moiety in **6b** to a greater than that in **6c**.

3.6. Oxidative Addition of H_2 to $[Rh(PH_3)_2(L)(HCOOH)]^+$ ($L = PH_3$ or H_2O). Since products of the H−OCOH reductive elimination, $[Rh(PH_3)_3(HCOOH)]^+$, **4a**, and $[Rh(PH_3)_2(H_2O)_2(HCOOH)]^+$, **4b**, have no hydride ligand, these complexes must undergo oxidative addition of H_2 to regenerate the active species, $[RhH_2(PH_3)_3]^+$, **1a**, and $[RhH_2(PH_3)_2(H_2O)]^+$, **1b**. In **4a**, approach of H_2 to the Rh center leads to $[Rh(PH_3)_3(\eta^2\text{-}H_2)(HCOOH)]^+$, **7a**, through transition state $\mathbf{TS_{4a-7a}}$, as shown in Figure 7. $\mathbf{TS_{4a-7a}}$ exhibits a small imaginary frequency (120i cm^{-1}), of which eigenvector mainly involves approach of H_2 to the Rh center. In $\mathbf{TS_{4a-7a}}$, the $Rh-H^\alpha$ and $Rh-H^\beta$ distances are about 2 Å, while the Rh−O bond considerably lengthens and formic acid moves downward from the $Rh(PH_3)_3$ plane. These geometry changes, as well as the eigenvector, suggest

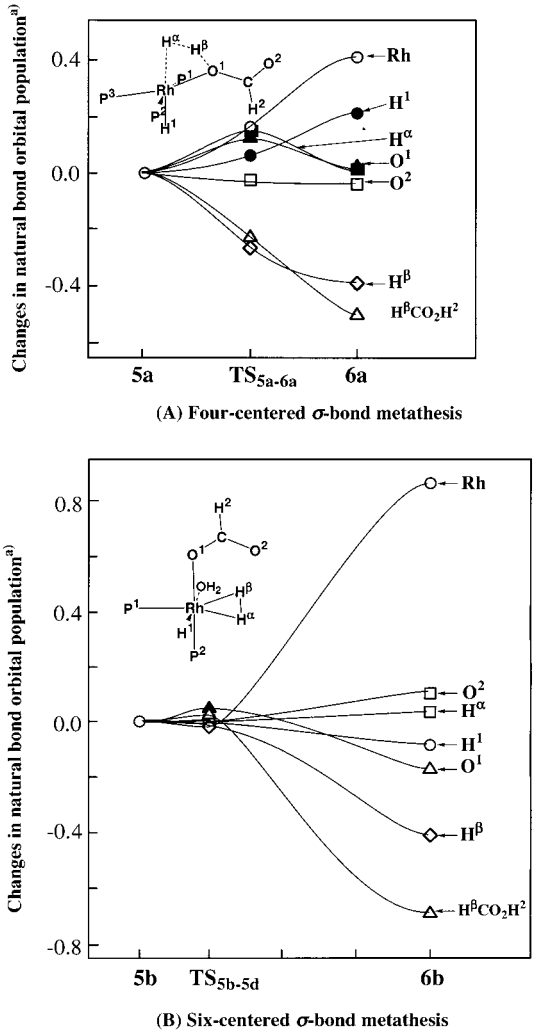

Figure 6. Population changes in the σ-bond metathesis of $[RhH(\eta^1\text{-OCOH})(PH_3)_2(L)]^+$ with H_2 (L = PH_3 or H_2O). (a) The natural bond orbital population[39] is determined with the DFT(B3LYP)/BS-II//DFT(B3LYP)/BS-I calculation. A positive value represents an increase in population relative to either **5a** in (A) or **5b** in (B).

that $\mathbf{TS_{4a-7a}}$ corresponds to substitution of formic acid for molecular hydrogen. In **7a**, the $H^\alpha-H^\beta$ bond (0.828 Å) is similar to those of **9c** (0.854 Å; see Figure 10) and $RhCl(PH_3)_2(\eta^2\text{-}H_2)$ (0.863 Å).[41] The activation barrier for $\mathbf{TS_{4a-7a}}$ was calculated to be 8.0 kcal/mol with the DFT(B3LYP)/BS-II method. The similar E_a values of 6.7 and 7.0 kcal/mol are calculated by MP4(SDQ) and CCSD(T) methods, respectively. HCOOH dissociates from **7a** to yield $[Rh(PH_3)_3(H_2)]^+$, **7c,** with a small destabilization energy of 4.4, 6.2, and 7.1 kcal/mol by DFT(B3LYP), MP4(SDQ), and CCSD(T) calculations, respectively. Consistent with the small energy destabilization, HCOOH dissociation induces little geometry changes of the $Rh(PH_3)_3(H_2)$ moiety.

From **7c**, the H_2 oxidative addition proceeds through $\mathbf{TS_{7c-1a}}$ to yield $[RhH_2(PH_3)_3]^+$, **1a**. In $\mathbf{TS_{7c-1a}}$, the $H^\alpha-H^\beta$ bond considerably lengthens, and the Rh−H bonds shorten to almost the same distance as those of **1a**. $\mathbf{TS_{7c-1a}}$ exhibits only one imaginary frequency (582i cm^{-1}), of which eigenvector mainly involves $H^\alpha-H^\beta$ bond breaking and $Rh-H^\beta$ bond formation. The activation barrier and the reaction energy are calculated to be 5.0 and −1.3 kcal/mol, respectively. The CCSD(T) method provides similar values (Table 3). This activation barrier is

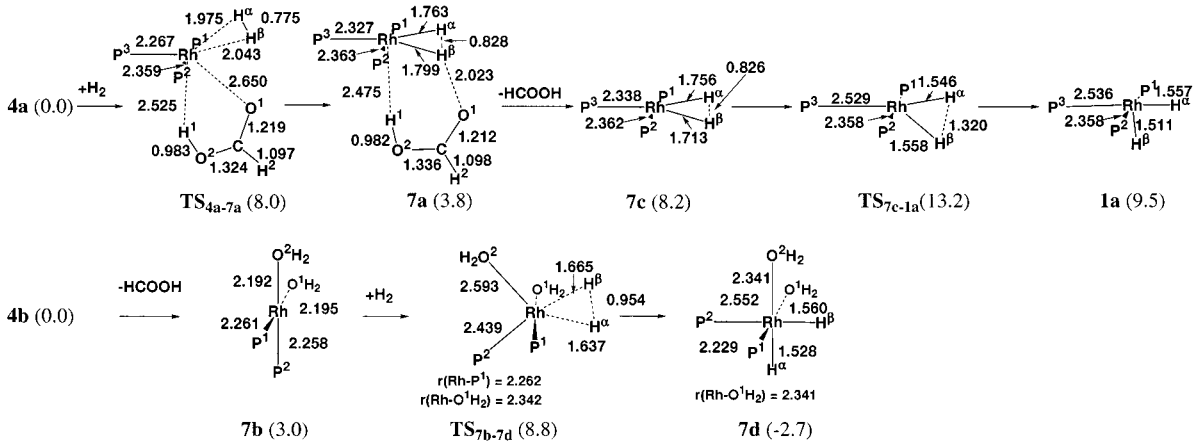

Figure 7. Geometry changes in the oxidative addition of H_2 to $[Rh(PH_3)_2(L)(HCOOH)]^+$ (L = PH_3 or H_2O). Bond distances are in Å. In parentheses are the energy differences from either **4a** (L = PH_3) or **4b** (L = H_2O) (kcal/mol unit; the DFT(B3LYP)/BS-II//DFT(B3LYP)/BS-I calculation).

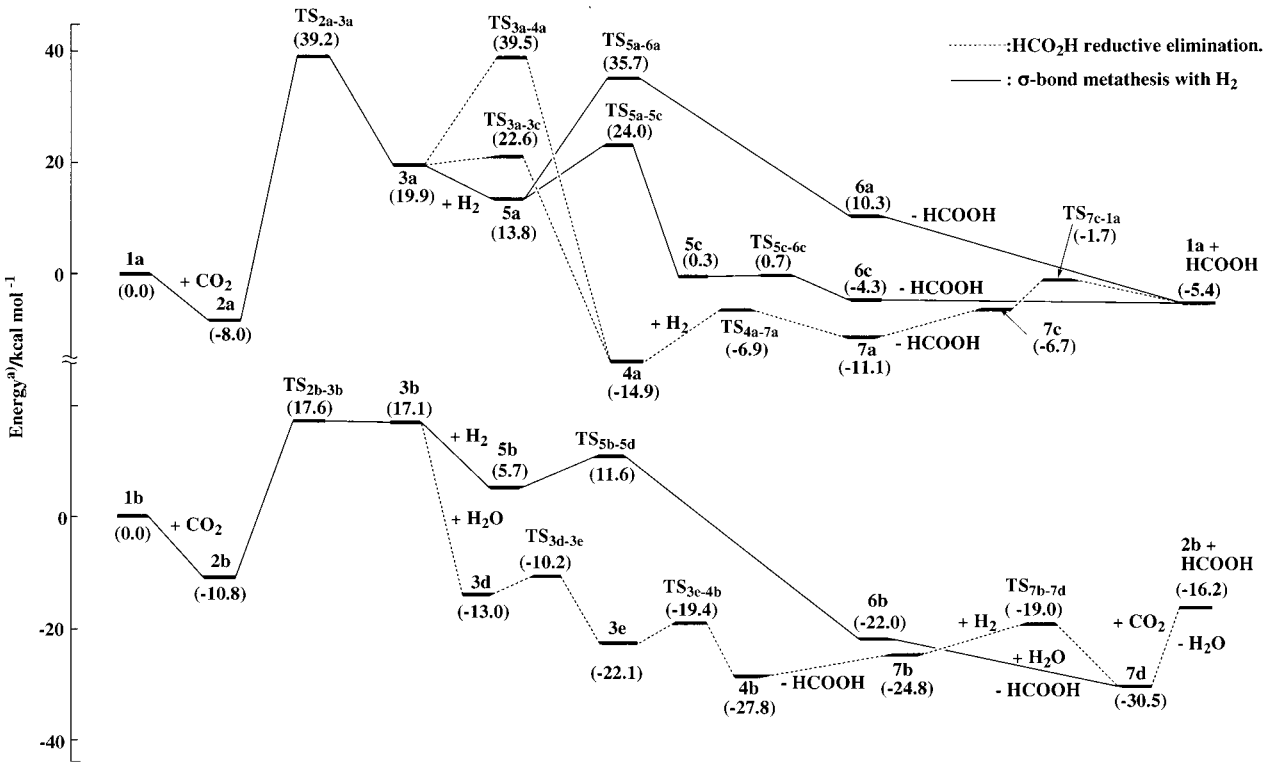

Figure 8. Energy changes in the $[RhH_2(PH_3)_2(L)]^+$-catalyzed hydrogenation of CO_2 into formic acid (L = PH_3 or H_2O). In parentheses are the energy differences from the sum of reactants (kcal/mol unit; the DFT(B3LYP)/BS-II//DFT(B3LYP)/BS-I calculation).

similar to the previously calculated value in the oxidative addition of H_2 to $RhCl(PH_3)_2$,[41] too.

In the case of **4b**, substitution of HCOOH for H_2O would easily occur, to afford $[Rh(PH_3)_2(H_2O)_2]^+$, **7b**, because H_2O is solvent. Oxidative addition of H_2 to **7b** occurs through the transition state $\mathbf{TS_{7b-7d}}$ in which the $H^{\alpha}-H^{\beta}$ distance (0.954 Å) is shorter than that in $\mathbf{TS_{7c-1a}}$ and the Rh−H bonds are longer than those of $\mathbf{TS_{7c-1a}}$. These features indicate that $\mathbf{TS_{7b-7d}}$ is relatively reactant-like compared to $\mathbf{TS_{7c-1a}}$. $\mathbf{TS_{7b-7d}}$ exhibits only one imaginary frequency (210i cm^{-1}), of which eigenvector mainly involves $H^{\alpha}-H^{\beta}$ bond breaking and Rh−H bond formation. The activation barrier is calculated to be 5.8, 2.9, and 4.1 kcal/mol by DFT(B3LYP), MP4(SDQ), and CCSD(T) methods, respectively, and the reaction energy is −5.7, −10.8, and −9.5 kcal/mol by DFT(B3LYP), MP4(SDQ), and CCSD(T) methods, respectively. Though the DFT(B3LYP) method slightly overestimates the E_a value and somewhat underestimates the ΔE value, it can be concluded that oxidative addition of H_2 to both $[Rh(PH_3)_3(HCOOH)]^+$ and $[Rh(PH_3)_2(H_2O)_2]^+$ easily proceeds with a small activation barrier to regenerate the active species $[RhH_2(PH_3)_3]^+$ and $[RhH_2(PH_3)_2(H_2O)_2]^+$.

3.7. Energy Changes along the Catalytic Cycle of Hydrogenation of CO_2 into Formic Acid by $[RhH_2(PH_3)_2(L)]^+$ (L = PH_3 or H_2O). Summarizing the above results, we will investigate here the energy changes along whole catalytic cycle, as shown in Figure 8, where the DFT(B3LYP)-calculated energy changes are given since the DFT(B3LYP) method provides energy changes similar to those by the CCSD(T) method (see above and footnote 37). CO_2 insertion reactions in **1a,b** lead to **3a,b** with activation barriers of 47.2 and 28.4 kcal/mol,

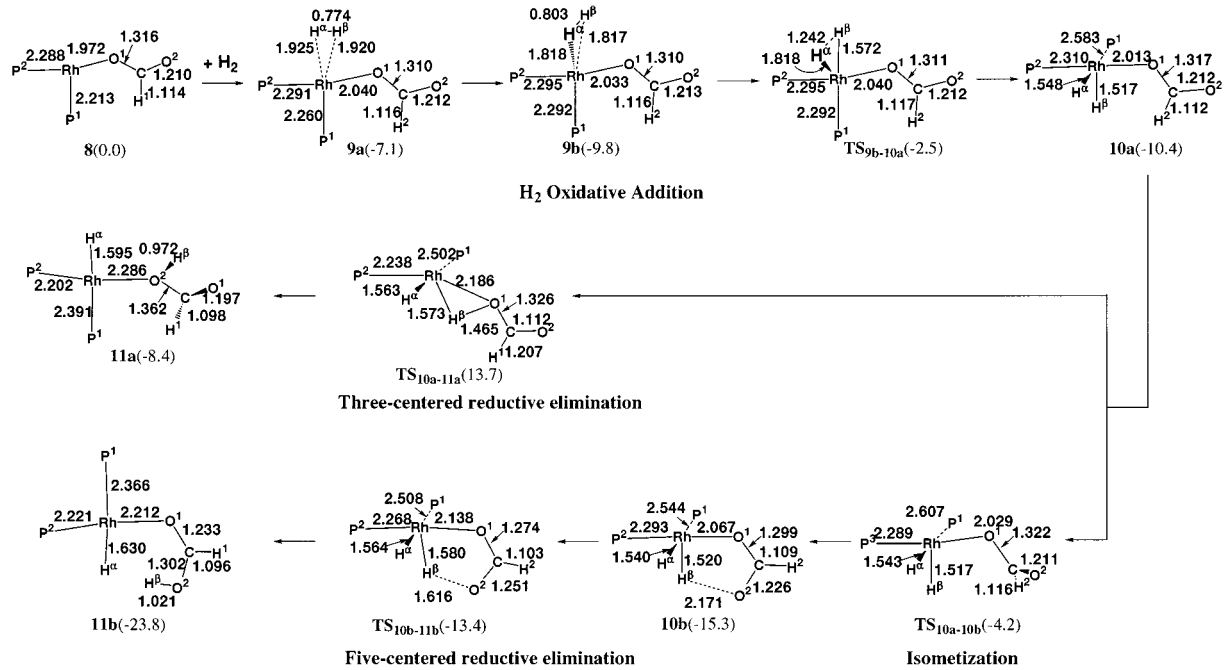

Figure 9. Geometry changes in the reductive elimination of formic acid from $RhH_2(\eta^1\text{-OCOH})(PH_3)_2$. Bond distances are in Å. In parentheses are the energy differences from **8** (kcal/mol unit; the DFT(B3LYP)/BS-II//DFT(B3LYP)/BS-I calculation).

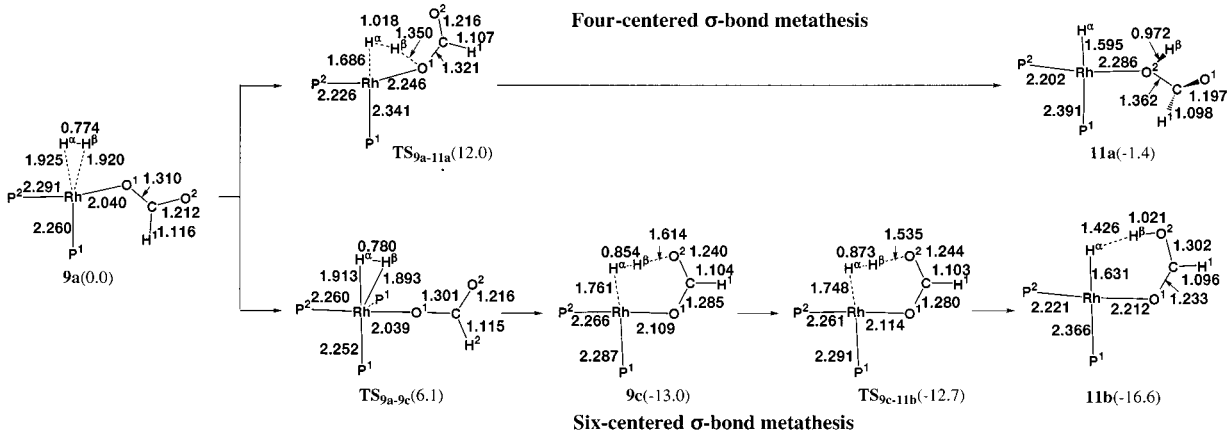

Figure 10. Geometry changes in the σ-bond metathesis of $Rh(\eta^1\text{-OCOH})(PH_3)_2$ with H_2. Bond distances are in Å. In parentheses are the energy differences from **9a** (kcal/mol unit; the DFT(B3LYP)/BS-II//DFT(B3LYP)/BS-I calculation).

Table 3. Activation Barrier (E_a) and Reaction Energy (ΔE) of Oxidative Addition of H_2 (**7c** → **1a** and **7b** → **7d**) (kcal/mol)[a]

	oxidative addition of H_2 (**7c** → **1a**)		oxidative addition of H_2 (**7b** → **7d**)	
	E_a	ΔE	E_a	ΔE
MP2	−1.3	−5.9	2.0	−14.1
MP3	4.1	−1.5	5.2	−9.5
MP4(DQ)	0.3	−5.0	3.3	−12.6
MP4(SDQ)	1.3	−2.8	2.9	−10.8
CCSD	3.2	−1.8	4.7	−9.2
CCSD(T)	3.0	−1.7	4.1	−9.5
DFT(B3LYP)	5.0	−1.3	5.8	−5.7
DFT(BLYP)	3.3	−0.4	5.3	−6.7
DFT(BP86)	2.5	−1.0	1.9	−10.1
DFT(BPW91)	2.6	−1.1	3.2	−8.7

[a] BS-II was used.

respectively. After **3a**, four reaction courses were investigated. However, two reaction courses through **TS$_{3a-4a}$** (three-centered H−OCOH reductive elimination) and **TS$_{5a-6a}$** (four-centered σ-bond metathesis) should be excluded because of their very large activation barriers. Thus, two possible reaction courses remain; in one course, the reaction proceeds through **3a** → **TS$_{3a-3c}$** → **4a** → **TS$_{4a-7a}$** → **7a** → **7c** → **TS$_{7c-1a}$** → **1a,** and in other one, the reaction proceeds through **3a** → **5a** → **TS$_{5a-5c}$** → **5c** → **TS$_{5c-6c}$** → **6c** → **1a**. Both reaction courses do not need large activation barrier, and the CO_2 insertion is the rate-determining step, as shown in Figure 8. After **3b**, two reaction courses were investigated, where the reaction courses through three-centered H−OCOH reductive elimination and four-centered σ-bond metathesis were excluded from the investigation because they needed large activation barrier. The reaction proceeds through **3b** → **3d** → **TS$_{3d-3e}$** → **3e** → **TS$_{3e-4b}$** → **4b** → **7b** → **TS$_{7b-7d}$** → **7d** → **2b** in one course and **3b** → **5b** → **TS$_{5b-5d}$** → **6b** → **7d** → **2b** in the other course. These two reaction courses do not need large activation barriers, too. Thus, the rate-determining step is CO_2 insertion in **1b**. Since the CO_2 insertion in **1a** needs a much larger activation barrier than that in **1b**, **1b** is an active species in the CO_2 hydrogenation reaction.

Though all the transition states (**TS$_{3d-3e}$**, **TS$_{3e-4b}$**, and **TS$_{7b-7d}$**) need moderate activation barriers in the reaction course through the five-centered reductive elimination and their values are similar to the activation barrier for **TS$_{5b-5d}$** in the reaction course through the six-centered σ-bond metathesis, the H_2O coordination to **3b** yields a large stabilization energy than the H_2 coordination. Thus, it should be clearly concluded that the best reaction course consists of the CO_2 insertion in **1b**, H_2O coordination, the **3d** → **3e** isomerization, the five-centered H−OCOH reductive elimination, and the oxidative addition of H_2. The other catalytic cycle is also possible, in which the reaction proceeds through the CO_2 insertion in **1b**, H_2 coordination, the **5b** → **5d** isomerization, and the six-centered σ-bond metathesis.

3.8. Catalytic Cycle of RhH(PH$_3$)$_2$-Catalyzed Hydrogenation of CO$_2$ into Formic Acid. We investigated six-centered transition state in the σ-bond metathesis of Rh(η^1-OCOH)(PH$_3$)$_2$-(H_2), **9a**, and five-centered transition state in the H−OCOH reductive elimination of RhH$_2$(η^1-OCOH)(PH$_3$)$_2$, **10a**, since these transition states have not been investigated yet. As shown in Figure 9, oxidative addition of H_2 to Rh(η^1-OCOH)(PH$_3$)$_2$, **8**, occurs through **TS$_{9b-10a}$** with a moderate activation barrier of 7.3 kcal/mol to afford **10a**. From **10a**, three-centered reductive elimination proceeds through **TS$_{10a-11a}$**, to afford RhH(PH$_3$)$_2$-(HCOOH), **11a**. This reductive elimination takes place with a considerably large activation barrier (24.1 kcal/mol), as reported previously.[13a] To achieve five-centered reductive elimination, **10a** must isomerize to **10b** in which the O^2 atom of formate takes a position in the same side of the H^β atom, as shown in Figure 9. This **10a** → **10b** isomerization occurs through **TS$_{10a-10b}$** with a moderate activation barrier of 6.2 kcal/mol. From **10b**, the five-centered H−OCOH reductive elimination occurs through **TS$_{10b-11b}$** with a very small activation barrier of 1.9 kcal/mol, to yield RhH(PH$_3$)$_2$(HCOOH), **11b**. The three-centered reductive elimination of **10b** also proceeds through **TS$_{10b-11a}$**, to afford RhH(PH$_3$)$_2$(HCOOH), **11a**, while a very large activation barrier of 24.2 kcal/mol is required, too. The complex **9a** undergoes the four-centered σ-bond metathesis through **TS$_{9a-11a}$** with a moderate activation barrier of 12.0 kcal/mol, to afford **11a**, as shown in Figure 10. If **9a** isomerizes to **9c**, six-centered σ-bond metathesis can take place. This isomerization occurs through **TS$_{9a-9c}$** with a moderate activation barrier of 6.1 kcal/mol, and then the six-centered σ-bond metathesis takes place through **TS$_{9c-11b}$** with nearly no barrier (E_a = 0.3 kcal/mol), to yield **11b**. From these results, it should be concluded that RhH(PH$_3$)$_2$-catalyzed hydrogenation of CO_2 proceeds through the CO_2 insertion into the Rh(I)−H bond to yield Rh(η^1-OCOH)(PH$_3$)$_2$, followed by two kinds of reaction courses; in one course, the H_2 oxidative addition to Rh(η^1-OCOH)(PH$_3$)$_2$ occurs to yield *cis*-RhH$_2$(η^1-OCOH)(PH$_3$)$_2$, and the isomerization of this complex takes place, followed by the five-centered H−OCOH reductive elimination. In the other course, the six-centered σ-bond metathesis of Rh(η^1-OCOH)-(PH$_3$)$_2$(H_2) occurs after the isomerization of Rh(η^1-OCOH)-(PH$_3$)$_2$(H_2). The rate-determining step is either the H_2 oxidative addition (E_a = 7.3 kcal/mol) in the former reaction course or the **9a** → **9c** isomerization (E_a = 6.1 kcal/mol) in the latter course.

3.9. Comparisons among Rhodium(I), Rhodium(III), and Ruthenium(II) Complexes in the CO$_2$ Hydrogenation into Formic Acid. Now, we have made all the preparations to make comparisons among rhodium(III), rhodium(I), and ruthenium-(II) complexes. One of the significant differences is observed in the CO_2 insertion reaction, as follows: The CO_2 insertion into the Rh(I)−H bond easily occurs with nearly no barrier, and the CO_2 insertion into the Ru(II)−H bond occurs with a moderate activation barrier (10.3 kcal/mol), while the CO_2 insertion into the Rh(III)−H bond needs a considerably large activation barrier (28−50 kcal/mol). We will first investigate the reason from the point of view of bond energies. In the CO_2 insertion into the M−H bond, the M−H bond is broken but the M−η^1-OCOH and C−H bonds are formed. We evaluated the H−H, Rh(I)−H, Rh(III)−H, and Ru(II)−H bond energies, considering the following equations:

$$H_2 \rightarrow H^\bullet + {}^\bullet H \tag{5}$$

$$\Delta E_{r-l}^{(5)} = D_e(H-H) \tag{6}$$

$$[Rh(PH_3)_2(L)_2]^+ + H_2 \rightarrow cis\text{-}[RhH_2(PH_3)_2(L)_2]^+ \tag{7}$$

$$\Delta E_{r-l}^{(7)} = D_e(H-H) - \Delta_e(Rh(III)-H^\alpha) - D_e(Rh(III)-H^\beta) \tag{8}$$

$$RhH(PH_3)_2 + H_2 \rightarrow cis\text{-}RhH_3(PH_3)_2 \tag{9}$$

$$\Delta E_{r-l}^{(9)} = D_e(Rh(I)-H) + D_e(H-H) - 2D_e(Rh(III)-H^\alpha) - D_e(Rh(III)-H^\beta) \tag{10}$$

$$Ru(PH_3)_4 + H_2 \rightarrow cis\text{-}RuH_2(PH_3)_4 \tag{11}$$

$$\Delta E_{r-l}^{(11)} = D_e(H-H) - 2D_e(Ru(II)-H^\alpha) \tag{12}$$

$$Ru(PH_3)_3 + H_2 \rightarrow cis\text{-}RuH_2(PH_3)_3 \tag{13}$$

$$\Delta E_{r-l}^{(13)} = D_e(H-H) - D_e(Ru(II)-H^\alpha) - D_e(Ru(II)-H^\beta) \tag{14}$$

$$(L = PH_3 \text{ or } H_2O)$$

Here D_e(X−Y) is the X−Y bond energy and ΔE_{r-l} is the difference in total energy (E_t) between the right- and the left-hand sides of the equation (see **1a** in Figure 7 for H^α and H^β). These bond energies were calculated with the MP2−MP4(SDQ), CCSD(T), and DFT(B3LYP) methods. As shown in Table 4, the Rh(I)−H bond is as strong as the Rh(III)−H bond, while the Ru(II)−H bond is stronger than both Rh(I)−H and Rh(III)−H bonds by ca. 10 kcal/mol.[42] These results indicate that the Rh(III)−H and Rh(I)−H bond strengths are not responsible for the much larger activation barrier of the CO_2 insertion into the Rh(III)−H bond than that of the CO_2 insertion into the Rh(I)−H bond. To find what factor determines the reactivity of CO_2 insertion reaction, we evaluated the O−H, Rh(I)−η^1-OCOH, Rh(III)−η^1-OCOH, and Ru(II)−η^1-OCOH bond energies, using the following equations:

$$HCOOH \rightarrow HCOO^\bullet + {}^\bullet H \tag{15}$$

$$\Delta E_{r-l}^{(15)} = D_e(O-H) \tag{16}$$

$$[RhH(\eta^1\text{-OCOH})(PH_3)_2(L)_n]^+ + H_2 \rightarrow [RhH_2(PH_3)_2(L)_n]^+ + HCOOH \quad (17)$$

$$\Delta E_{r-l}^{(17)} = D_e(Rh(III)-\eta^1\text{-OCOH}) + D_e(H-H) - D_e(Rh(III)-H^\alpha) - D_e(O-H) \quad (18)$$

$$Rh(\eta^1\text{-OCOH})(PH_3)_2 + H_2 \rightarrow RhH(PH_3)_2 + HCOOH \quad (19)$$

$$\Delta E_{r-l}^{(19)} = D_e(Rh(I)-\eta^1\text{-OCOH}) + D_e(H-H) - D_e(Rh(I)-H) - D_e(O-H) \quad (20)$$

$$RuH(\eta^1\text{-OCOH})(PH_3)_3 + H_2 \rightarrow RuH_2(PH_3)_3 + HCOOH \quad (21)$$

$$\Delta E_{r-l}^{(21)} = D_e(Ru(II)-\eta^1\text{-OCOH}) + D_e(H-H) - D_e(Ru(II)-H^\alpha) - D_e(O-H) \quad (22)$$

$$(L = PH_3 \text{ or } H_2O;\ n = 1 \text{ or } 2)$$

As shown in Table 4, the Rh(I)−η^1-OCOH and Ru(II)−η^1-OCOH bonds are considerably stronger than the Rh(III)−η^1-OCOH bond by 20−29 and 33−45 kcal/mol, respectively. Thus, the stronger Rh(I)−η^1-OCOH and Ru(II)−η^1-OCOH bonds than the Rh(III)−η^1-OCOH bond are responsible for the fact that CO_2 is much more easily inserted into the Rh(I)−H and Ru(II)−H bonds than that into the Rh(III)−H bond. Though the Ru(II)−η^1-OCOH bond is stronger than the Rh(I)−η^1-OCOH bond by 16 kcal/mol (CCSD(T) calculation), the Ru(II)−H bond is stronger than the Rh(I)−H bond by 14 kcal/mol. This stronger Ru(II)−H bond is one of the factors leading to the larger activation barrier of the CO_2 insertion into the Ru(II)−H bond than that into the Rh(I)−H bond (the other reason such as HOMO energy level will be discussed below). To investigate the reason that the Rh(III)−η^1-OCOH bond is the weakest, we inspected electron population of the η^1-OCOH moiety, as shown in Table 5. Apparently, the η^1-OCOH moiety is the least negatively charged in $[RhH(\eta^1\text{-OCOH})(PH_3)_3]^+$ but most negatively charged in $RuH(\eta^1\text{-OCOH})(PH_3)_3$. The electron affnity (EA) of OCOH was calculated to be 3.49, 3.35, 3.04, and 3.44 eV with the DFT(B3LYP), MP4(SDQ), CCSD(T), and G2MP2 methods, respectively. This positive EA value clearly indicates that the more electrons the OCOH moiety receives from the metal moiety, the more stable the M−η^1-OCOH bond becomes.

Table 4. M−R Bond Energies[a] (M = Rh(I), Rh(III), or Ru(II), R = H or η^1-OCOH) (kcal/mol)

	D_e(Rh(I)–H)	D_e(Rh(III)–H)	D_e(Ru(II)–H)
MP2	61.7	57.3 (59.8)	69.3
MP3	54.5	56.8 (57.4)	73.4
MP4(DQ)	60.1	58.7 (60.6)	71.7
MP4(SDQ)	60.1	57.9 (59.5)	69.6
CCSD	56.9	57.3 (58.5)	72.7
CCSD(T)	58.0	57.4 (59.0)	72.4
DFT(B3LYP)	57.3	57.8 (58.3)	71.3
	D_e(Rh(I)–η^1-OCOH)	D_e(Rh(III)–η^1-OCOH)	D_e(Ru(II)–η^1-OCOH)
MP2	90.7	69.1 (63.0)	101.8
MP3	78.9	59.2 (50.6)	102.8
MP4(DQ)	80.5	58.8 (51.4)	95.5
MP4(SDQ)	80.8	59.6 (52.3)	93.5
CCSD	74.6	53.8 (46.2)	94.0
CCSD(T)	76.8	54.7 (47.4)	92.3
DFT(B3LYP)	63.0	45.2 (37.4)	78.9

[a] BS-II was used. [b] In parentheses are the bond energies which are calculated at L = PH_3 and n = 1.

Table 5. NBO Charge (ρ)[a] of the η^1-OCOH Moiety in $[RhH(\eta^1\text{-OCOH})(PH_3)_3]^+$, $[RhH(\eta^1\text{-OCOH})(PH_3)_2(H_2O)]^+$, $[RhH(\eta^1\text{-OCOH})(PH_3)_2(H_2O)_2]^+$, $Rh(\eta^1\text{-OCOH})(PH_3)_2$, and $RuH(\eta^1\text{-OCOH})(PH_3)_3$ and the Energy of the Frontier Orbital Involving H 1s and Rh dσ Orbitals in $[RhH_2(PH_3)_3]^+$, $[RhH_2(PH_3)_2(H_2O)]^+$, $[RhH_2(PH_3)_2(H_2O)_2]^+$, $RhH(PH_3)_2$, and $RuH_2(PH_3)_3$

		$\epsilon\phi$(H 1s + λdσ)[b]	
	$\rho(\eta^1\text{-OCOH})$[a] (e)	HF (eV)	DFT(B3LYP) (eV)
$[RhH(\eta^1\text{-OCOH})(PH_3)_3]^+$	−0.42	−15.02	−12.27
$[Rh(\eta^1\text{-OCOH})(PH_3)_2(H_2O)]^+$	−0.34	−14.96	−12.30
$[Rh(\eta^1\text{-OCOH})(PH_3)_2(H_2O)_2]^+$	−0.54	−14.45	−11.66
$Rh(\eta^1\text{-OCOH})(PH_3)_2$	−0.54	−9.71	−7.23
$RuH(\eta^1\text{-OCOH})(PH_3)_3$	−0.58	−9.24	−6.61

[a] The natural bond orbital population[39] analysis was carried out with the DFT(B3LYP)/BS-II//DFT(B3LYP)/BS-I method. Neutral OCOH has 23.00 electrons. [b] DFT(B3LYP)/BS-II//DFT(B3LYP)/BS-I calculations. The LCAO coeffcient λ is much smaller than 1.0.

In other words, the more electron donating the metal moiety is, the more stable the M−OCOH moiety is formed. The Ru(II) and Rh(I) moieties can supply enough electrons to η^1-OCOH, since both Ru(II) and Rh(I) are electron-rich. However, the Rh(III) moiety is short of electron density and therefore it cannot supply enough electrons to η^1-OCOH. Hence, the Rh(III)−η^1-OCOH moiety becomes less stable than the other ones.

The charge transfer from metal to CO_2 also plays an important role in the CO_2 insertion into the M−H bond.[43] The frontier orbital which participates in the charge transfer mainly consists of H 1s and metal d orbitals. This orbital becomes higher in energy in the order $[RhH_2(PH_3)_3]^+ < RhH(PH_3)_2 < RuH_2(PH_3)_3$, as shown in Table 5. Because of these frontier orbital energies, the charge transfer from the metal hydride moiety to CO_2 becomes weaker in the order Ru(II) > Rh(I) > Rh(III) and the activation barrier of the CO_2 insertion increases in the order Ru(II) < Rh(I) < Rh(III). Thus, the large activation barrier of the CO_2 insertion into the Rh(III)−H bond is reasonably understood in terms of the weak charge transfer from the Rh(III)−H moiety to CO_2. Against this expectation, the CO_2 insertion into the Ru(II)−H bond needs a larger activation barrier than the insertion into the Rh(I)−H bond. This is probably because the Ru(II)−H bond is much stronger than the Rh(I)−H bond, as mentioned above.

(42) All the M−H bond energies moderately fluctuate upon going from MP2 to DFT in Table 4. Thus, it is reasonably suggested that MP2 and DFT methods evaluate correctly the Rh−H bond energy. This means that all the computational methods adopted here provide reliable results of $[RhH_2(PH_3)_2(H_2O)]^+$, $[RhH_2(PH_3)_3]^+$, $RhH(PH_3)_2$, $RuH_2(PH_3)_3$, and H. However, the MP2 method provides the larger M−O bond energy but the DFT method provides the smaller M−O bond energy than does the CCSD(T) method, as shown in Table 4. These results suggest that M−(η^1-OCOH) and/or $OCOH^-$ species cannot be calculated reliably by the MP2 method. To ascertain this suggestion, we estimated the H−OCOH bond energy by MP2-MP4(SDQ), CCSD(T), DFT, and G2MP2 methods. As discussed in footnote 37, the MP2-MP4(SDQ) methods overestimate the H−OCOH bond energy but both CCSD(T) and DFT methods provide a H−OCOH bond energy similar to that of the G2MP2 method. These results suggest that the DFT method is more reliable than the MP2-MP4(SDQ) methods in the calculation of the OCOH ligand. Also, it is noted that the MP2-MP4(SDQ) methods would overestimate the activation barrier and underestimate the reaction energy of the H−OCOH reductive elimination and the σ-bond metathesis.

(43) Sakaki, S.; Musashi, Y. *Inorg. Chem.* **1995**, *34*, 1914.

Table 6. Activation Barrier (E_a) and Reaction Energy (ΔE) of Five-Centered H−OCOH Reductive Elimination and Six-Centered σ-Bond Metathesis with Molecular Dihydrogen in $[RhH(\eta^1\text{-}OCOH)(PH_3)_2(L)_n]^+$ (L = PH_3 or H_2O, n = 1 or 2), $RhH(\eta^1\text{-}OCOH)(PH_3)_2$, and $RuH(\eta^1\text{-}OCOH)(PH_3)_3$ (DFT(B3LYP)/BS-II; kcal/mol)

	five-centered H–OCOH reductive elimination		six-centered σ-bond metathesis	
	E_a	ΔE	E_a	ΔE
$[RhH(\eta^1\text{-}OCOH)(PH_3)_3]^+$	no[a]	−34.8	0.4	−4.6
$[RhH(\eta^1\text{-}OCOH)(PH_3)_2(H_2O)_2]^+$	2.7	−5.7	5.9[c]	−27.7[c]
$Rh(\eta^1\text{-}OCOH)(PH_3)_2$	1.9[b]	−8.5[b]	0.3	−3.6
$RuH(\eta^1\text{-}OCOH)(PH_3)_3$	17.5	17.9	8.2	7.8

[a] The five-centered H OCOH reductive elimination from $[RhH(\eta^1\text{-}OCOH)(PH_3)_3]^+$ occurs with no barrier. [b] E_a and ΔE values of five-centered reductive elimination of $RhH_2(\eta^1\text{-}OCOH)(PH_3)_2$. [c] E_a and ΔE values of six-centered σ-bond metathesis of $[RhH(\eta^1\text{-}OCOH)(PH_3)_2(H_2O)(H_2)]^+$.

In the ruthenium(II)-catalyzed hydrogenation of CO_2, not PPh_3 but PMe_3 was used as a ligand, to enhance the solubility of the ruthenium(II) complex.[12] However, PMe_3 is favorable not only from viewpoint of the solubility but also from the viewpoint of donating ability, since PMe_3 pushes up the metal d orbital in energy. This is considered one of the reasons that $RuX_2(PMe_3)_4$ exhibits very high catalytic activity.

The other important difference among rhodium(I), rhodium(III), and ruthenium(II) complexes is that the six-centered σ-bond metathesis more easily takes place than the five-centered H−OCOH reductive elimination in $RuH(\eta^1\text{-}OCOH)(PH_3)_3$, while both reactions occur easily in $[RhH(\eta^1\text{-}OCOH)(PH_3)_3]^+$ and $RhH_2(\eta^1\text{-}OCOH)(PH_3)_2$, as compared in Table 6. This difference is interpreted in terms of the M−H bond strength. The M−H bond should be broken in the reductive elimination, while the M−H bond is formed in the σ-bond metathesis. Since the Ru(II)−H bond is much stronger than the Rh(I)−H and Rh(III)−H bonds, the σ-bond metathesis more easily occurs than the reductive elimination in $RuH(\eta^1\text{-}OCOH)(PH_3)_3$.

4. Conclusions

Conclusions presented in this work are summarized as follows: (1) Not $[RhH_2(PH_3)_3]^+$ but $[RhH_2(PH_3)_2(H_2O)]^+$ is an active species in Rh(III)-catalyzed hydrogenation of CO_2 into formic acid. (2) The first step is the CO_2 insertion into the Rh(III)−H bond (E_a = 28 kcal/mol) of $[RhH_2(PH_3)_2(H_2O)]^+$. (3) After the insertion reaction, two reaction courses are possible: In one course, the reaction proceeds through H_2O coordination to $[RhH(\eta^1\text{-}OCOH)(PH_3)_2(H_2O)]^+$, the isomerization of $[RhH(\eta^1\text{-}OCOH)(PH_3)_2(H_2O)_2]^+$ (E_a = 3 kcal/mol), the five-centered H−OCOH reductive elimination (E_a = 3 kcal/mol), and the oxidative addition of molecular dihydrogen to $[Rh(PH_3)_2(H_2O)_2]^+$ (E_a = 6 kcal/mol). In the other course, the six-centered σ-bond metathesis of $[RhH(\eta^1\text{-}OCOH)(PH_3)_2(H_2O)(H_2)]^+$ occurs with no barrier after the isomerization of $[RhH(\eta^1\text{-}OCOH)(PH_3)_2(H_2O)(H_2)]^+$ (E_a = 6 kcal/mol). (4) The former reaction course is more favorable than the latter, since H_2O coordination occurs with a larger stabilization energy than H_2 coordination. And (5) the rate-determining step is the CO_2 insertion into the Rh(III)−H bond in both reaction courses.

DFT(B3LYP) calculations show that two reaction mechanisms are possible in the rhodium(I)-catalyzed CO_2 hydrogenation: In one mechanism, the reaction proceeds through the CO_2 insertion into the Rh(I)−H bond ($E_a \sim 0$ kcal/mol), the isomerization of $Rh(\eta^1\text{-}OCOH)(PH_3)_2(H_2)$ (E_a = 6 kcal/mol), and the six-centered σ-bond metathesis of $Rh(\eta^1\text{-}OCOH)(PH_3)_2(H_2)$ ($E_a \sim 0$ kcal/mol). In the other mechanism, the reaction proceeds through the CO_2 insertion, the oxidative addition of H_2 to $Rh(\eta^1\text{-}OCOH)\text{-}(PH_3)_2$ (E_a = 7 kcal/mol) to yield $RhH_2(\eta^1\text{-}OCOH)(PH_3)_2$, the isomerization of $RhH_2(\eta^1\text{-}OCOH)(PH_3)_2$ (E_a = 6 kcal/mol), and the five-centered H−OCOH reductive elimination ($E_a \sim 0$ kcal/mol) of $RhH_2(\eta^1\text{-}OCOH)(PH_3)_2$. The rate-determining step is the isomerization of the rhodium formate complex in both mechanisms.

One of the interesting differences among the rhodium(I), ruthenium(II), and rhodium(III) complexes is observed in the CO_2 insertion step. The CO_2 insertion into the Rh(I)−H and the Ru(II)−H bonds easily occurs with nearly no barrier and a moderate activation barrier, respectively, while the CO_2 insertion into the Rh(III)−H bond occurs with a very large activation barrier. Since the charge transfer from the M−H moiety to CO_2 plays an important role in the CO_2 insertion reaction, the CO_2 insertion easily takes place when the HOMO of the metal−hydride complex is at a high energy. Also, the M−η^1-OCOH bond becomes strong, when the metal moiety is electron-rich. From the above discussion, we wish to predict that the donating ligand should be used in the metal complex when the CO_2 insertion is a rate-determining step. Also, we recommend to use the early transition metal complex, since the d orbital becomes higher in energy upon going to the left-hand side from the right-hand side in the periodic table. Such attempt has not been tried yet to our knowledge. The CO_2 hydrogenation with early transition metal complexes is under theoretical investigation now.

Acknowledgment. All the calculations were carried out with the FUJITSU VPP5500 of the Research Center for Computational Science, Okazaki National Research Institutes (Okazaki, Japan) and COMPAQ-Alpha 600au in our laboratory. This work was financially supported in part by the Grant-in-Aid for Scientific Research on Priority Areas "Molecular Physical Chemistry" from the Ministry of Education, Culture, Sports, and Science of Japan (No. 403).

Supporting Information Available: Figures of the eigenvectors with imaginary frequency (DFT(B3LYP)/BS-I) in the transition states of the CO_2 insertion into the Rh(III)−H bond of *cis*-$[RhH_2(PH_3)_2(L)]^+$ (L = PH_3 or H_2O) (**TS$_{2a-3a}$** and **TS$_{2b-3b}$**), the isomerization of $[RhH(\eta^1\text{-}OCOH)(PH_3)_2(L)_n]^+$ (n = 1 and 2) (**TS$_{3a-3c}$** and **TS$_{3d-3e}$**), the H−OCOH reductive elimination of $[RhH(\eta^1\text{-}OCOH)(PH_3)_2(L)]^+$ (**TS$_{3a-4a}$** and **TS$_{3e-4b}$**), the σ-bond metathesis of $[RhH(\eta^1\text{-}OCOH)(PH_3)_3(H_2)]^+$ (**TS$_{5a-6a}$** and **TS$_{5c-6c}$**), the isomerization of $[RhH(\eta^1\text{-}OCOH)(PH_3)_2(L)\text{-}(H_2)]^+$ (L = PH_3 or H_2O) (**TS$_{5a-5c}$**, **TS$_{5b-5d}$**, and **TS$_{5e-5f}$**), the dissociative substitution of H_2 for H_2 in $[RhH(\eta^1\text{-}OCOH)(PH_3)_3\text{-}(H_2)]^+$ (**TS$_{5a-5e}$**), the substitution of H_2 for HCOOH in $[Rh\text{-}(PH_3)_3(HCOOH)]^+$ (**TS$_{4a-7a}$**), the oxidative addition of H_2 to $[Rh(PH_3)_3]^+$ (**TS$_{7c-1a}$**), the oxidative addition of H_2 to $[Rh\text{-}(PH_3)_2(H_2O)_2]^+$ (**TS$_{7b-7d}$**), the oxidative addition of H_2 to $Rh(\eta^1\text{-}OCOH)(PH_3)_2$ (**TS$_{9b-10a}$**), the H−OCOH reductive elimination of $RhH_2(\eta^1\text{-}OCOH)(PH_3)_2$ (**TS$_{10a-11a}$** and **TS$_{10b-11b}$**), the isomerization of $RhH_2(\eta^1\text{-}OCOH)(PH_3)_2$ (**TS$_{10a-10b}$**), the σ-bond metathesis of $Rh(\eta^1\text{-}OCOH)(PH_3)_2(H_2)$ (**TS$_{9a-11a}$** and **TS$_{9c-11b}$**), and the isomerization of $Rh(\eta^1\text{-}OCOH)(PH_3)_2(H_2)$ (**TS$_{9a-9c}$**), figures of energy changes (DFT(B3LYP)/BS-II) in the five-centered H−OCOH reductive elimination of $[RhH(\eta^1\text{-}OCOH)\text{-}(PH_3)_3]^+$, figures of population changes in the three-centered

H−OCOH reductive elimination (**3a** → **4a** via $\mathbf{TS_{3a-4a}}$), the five-centered H−OCOH reductive elimination (**3a** → **4a** via $\mathbf{TS_{3a-3c}}$), the four-centered σ-bond metathesis (**5a** → **6a**), the six-centered σ-bond metathesis (**5a** → **6c**), the four-centered σ-bond metathesis (**5a** → **6a**), and the four-centered σ-bond metathesis (**5c** → **6c**), figures of three-dimensional (3D) maps of frontier orbitals of $HCOO^-$, transition states in the H−OCOH reductive elimination, and σ-bond metathesis, Cartesian coordinates for all the intermediates and transition states, and results of an instability calculation of a single-determinant DFT function at the transition state (PDF). This material is available free of charge via the Internet at http://pubs.acs.org.

JA020063C